JOURNAL OF GEOPHYSICAL RESEARCH: SOLID EARTH, VOL. 118, 6049–6065, doi:10.1002/2013JB010381, 2013

Low-temperature magnetic properties of pelagic carbonates: Oxidation of biogenic magnetite and identification of magnetosome chains

Liao Chang,[1,2] Michael Winklhofer,[3] Andrew P. Roberts,[2] David Heslop,[2] Fabio Florindo,[4] Mark J. Dekkers,[1] Wout Krijgsman,[1] Kazuto Kodama,[5] and Yuhji Yamamoto[5]

Received 24 May 2013; revised 19 August 2013; accepted 24 October 2013; published 11 December 2013.

[1] Pelagic marine carbonates provide important records of past environmental change. We carried out detailed low-temperature magnetic measurements on biogenic magnetite-bearing sediments from the Southern Ocean (Ocean Drilling Program (ODP) Holes 738B, 738C, 689D, and 690C) and on samples containing whole magnetotactic bacteria cells. We document a range of low-temperature magnetic properties, including reversible humped low-temperature cycling (LTC) curves. Different degrees of magnetite oxidation are considered to be responsible for the observed variable shapes of LTC curves. A dipole spring mechanism in magnetosome chains is introduced to explain reversible LTC curves. This dipole spring mechanism is proposed to result from the uniaxial anisotropy that originates from the chain arrangement of biogenic magnetite, similar to published results for uniaxial stable single domain (SD) particles. The dipole spring mechanism reversibly restores the remanence during warming in LTC measurements. This supports a previous idea that remanence of magnetosome chains is completely reversible during LTC experiments. We suggest that this magnetic fingerprint is a diagnostic indicator for intact magnetosome chains, although the presence of isolated uniaxial stable SD particles and magnetically interacting particles can complicate this test. Magnetic measurements through the Eocene section of ODP Hole 738B reveal an interval with distinct magnetic properties that we interpret to originate from less oxidized biogenic magnetite and enrichment of a biogenic "hard" component. Co-occurrence of these two magnetic fingerprints during the late Eocene in the Southern Ocean indicates less oxic conditions, probably due to increased oceanic primary productivity and organic carbon burial.

Citation: Chang, L., M. Winklhofer, A. P. Roberts, D. Heslop, F. Florindo, M. J. Dekkers, W. Krijgsman, K. Kodama, and Y. Yamamoto (2013), Low-temperature magnetic properties of pelagic carbonates: Oxidation of biogenic magnetite and identification of magnetosome chains, *J. Geophys. Res. Solid Earth*, *118*, 6049–6065, doi:10.1002/2013JB010381.

1. Introduction

[2] Pelagic carbonates occur in vast amounts on land in tectonically uplifted marine sedimentary sequences and are deposited on almost half of the world's ocean floor. They provide outstanding archives of paleoenvironmental change and paleomagnetic polarity patterns throughout significant parts of Earth history [e.g., *Roberts et al.*, 2013]. For example, paleomagnetic records from pelagic carbonates enable magnetostratigraphic calibration of biostratigraphic events that provide age control for sedimentary sequences [e.g., *Lowrie et al.*, 1980; *Florindo and Roberts*, 2005; *Channell et al.*, 2013]. Carbonate records also contribute to our understanding of past geomagnetic field behavior [e.g., *Valet and Meynadier*, 1993]. Recently, it has been demonstrated that biogenic magnetite (Fe_3O_4) produced by magnetotactic bacteria (MTB) makes a significant contribution to the magnetic signal in marine carbonates [e.g., *Tarduno*, 1994; *Tarduno et al.*, 1998; *Abrajevitch and Kodama*, 2009; *Yamazaki*, 2009, 2012; *Roberts et al.*, 2011a, 2012, 2013; *Chang et al.*, 2012a; *Larrasoaña et al.*, 2012; *Channell et al.*, 2013]. Biogenic magnetite crystals have a range of distinct properties, such as single domain (SD) magnetic behavior, narrow particle size distributions, characteristic crystal morphologies, and chain architecture [e.g., *Kopp and Kirschvink*, 2008]. Variations within this range of properties can potentially

[1]Paleomagnetic Laboratory "Fort Hoofddijk," Department of Earth Sciences, Utrecht University, Utrecht, Netherlands.
[2]Research School of Earth Sciences, The Australian National University, Canberra, Australia.
[3]Department of Earth and Environmental Sciences, Ludwig-Maximilians University, Munich, Germany.
[4]Istituto Nazionale di Geofisica e Vulcanologia, Rome, Italy.
[5]Center for Advanced Marine Core Research, Kochi University, Nankoku, Kochi, Japan.

Corresponding author: L. Chang, Research School of Earth Sciences, The Australian National University, Canberra, ACT 0200, Australia. (liao.chang@anu.edu)

©2013. American Geophysical Union. All Rights Reserved.
2169-9313/13/10.1002/2013JB010381

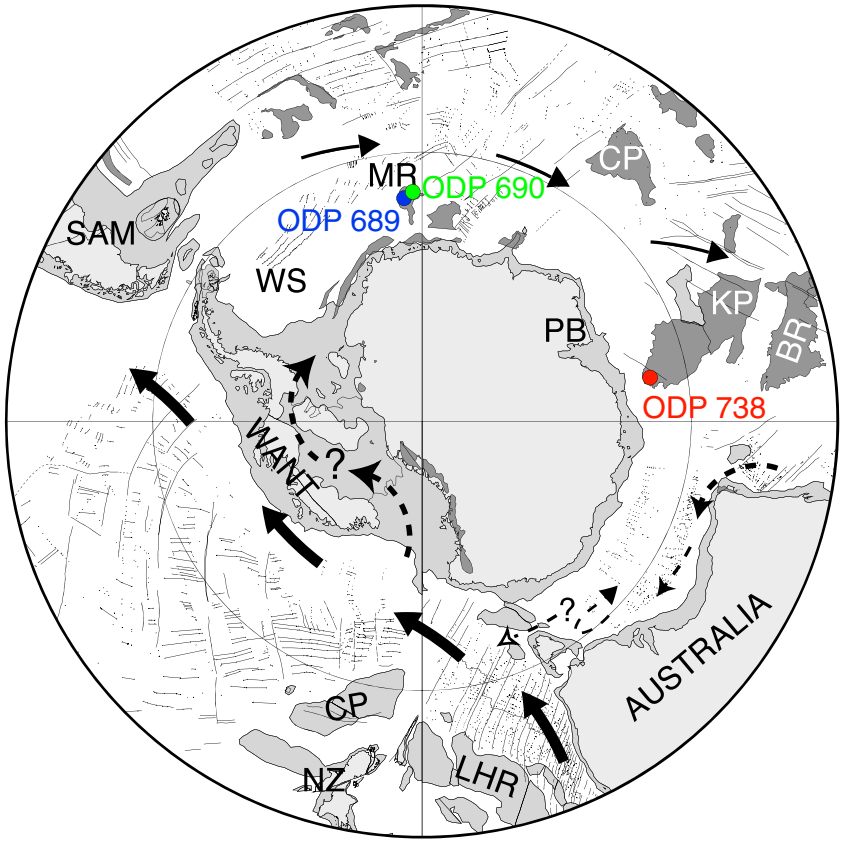

Figure 1. Plate reconstruction of the Southern Ocean during the late Eocene [after *Lawver and Gahagan*, 2003] and the locations of ODP Sites 738, 689, and 690 (polar stereographic projection to 45°S). Arrows indicate ocean currents. KP = Kerguelen Plateau, BR = Broken Ridge, CP (white) = Crozet Plateau, PB = Prydz Bay, MR = Maud Rise, WS = Weddell Sea, WANT = West Antarctica, SAM = South America, CP (black) = Campbell Plateau, NZ = New Zealand, and LHR = Lord Howe Rise.

reflect fluctuations in the relative balance and contribution of different species to the total MTB population and of environmental changes [*Egli*, 2004a, 2004b]. Therefore, the magnetic signatures of biogenic magnetite preserved in pelagic carbonates can be useful for paleomagnetic and paleoenvironmental reconstructions.

[3] The magnetic properties of pelagic carbonates at room temperature have been investigated extensively. In contrast, their low-temperature magnetic behavior is less well known because of a more limited number of studies [e.g., *Mauritsch and Turner*, 1975; *Lowrie and Heller*, 1982; *Smirnov and Tarduno*, 2000; *Housen and Moskowitz*, 2006; *Abrajevitch and Kodama*, 2009; *Roberts et al.*, 2012; *Yamazaki and Ikehara*, 2012]. Low-temperature magnetic analysis can provide important information in addition to room-temperature and high-temperature magnetic analyses. For example, low-temperature magnetic methods are widely used to identify magnetic minerals via their magnetic phase transitions, for quantifying superparamagnetic (SP) behavior, and for understanding the stability of remanence. Low-temperature magnetic analysis can be particularly useful when studying pelagic carbonates because their magnetic properties are often dominated by biogenic magnetite [e.g., *Roberts et al.*, 2012, 2013]. Magnetite is well known for its distinctive low-temperature magnetic properties across the Verwey transition (T_v) at ~120–125 K [*Verwey*, 1939] and the isotropic point at ~135 K [*Bickford et al.*, 1957]. The magnetic properties of magnetite are also sensitive to oxidation [e.g., *Özdemir et al.*, 1993; *Moskowitz et al.*, 1993; *Cui et al.*, 1994; *Torii*, 1997; *Smirnov and Tarduno*, 2000; *Özdemir and Dunlop*, 2010] and magnetostatic interactions [e.g., *Muxworthy and McClelland*, 2000]. We have carried out detailed low-temperature magnetic analyses on Eocene/Oligocene sediments from the Southern Ocean (Ocean Drilling Program (ODP) Holes 738B, 738C, 689D, and 690C), and on samples containing whole MTB cells and inorganic magnetic minerals. We report novel low-temperature magnetic properties of biogenic magnetite and provide an explanation for the observed range of magnetic properties. Our analysis provides new insights into the low-temperature magnetic properties of pelagic carbonates that will assist future paleomagnetic and environmental magnetic studies of such sediments.

2. Materials and Methods

[4] Detailed magnetic analyses were carried out on samples from ODP Hole 738B (62°42, 54′S; 82°47, 25′E; 2,253 m water depth; 1750 m paleo water depth), on the southern Kerguelen Plateau (SKP) and north of the modern

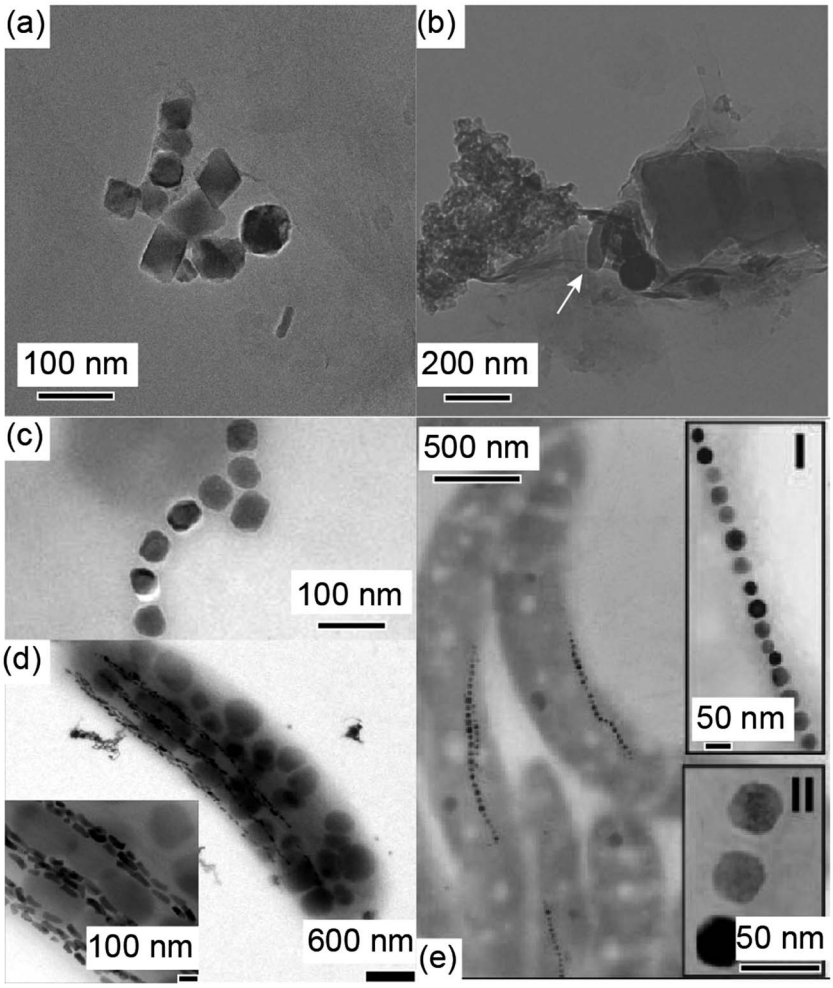

Figure 2. TEM images for (a, b) fossilized biogenic magnetite crystals extracted from pelagic carbonates (ODP Hole 738B), (c) magnetosome crystals from wild-type *Magnetospirillum magneticum* AMB-1, (d) a whole cell of uncultivated *Magnetobacterium bavaricum* MYR-1 with bullet-shaped magnetosomes, and (e) whole cells and magnetosomes of cultured *Magnetospirillum gryphiswaldense* MSR-1. In Figure 2a, some of the magnetofossil crystals have relatively well-preserved morphologies, while alteration is also evident around the edges of some grains. In Figure 2b, a bullet-shaped magnetofossil crystal is identified (arrow). In Figure 2e, I and II indicate a magnetite chain and high resolution image of magnetosome crystals, respectively. TEM images for Figures 2c, 2d, and 2e are from *Kopp et al*. [2006a], *Li et al*. [2010], and *Scheffel et al*. [2008], respectively.

Antarctic divergence and south of the Polar Frontal Zone (Figure 1). Samples from the late and middle Eocene portion of the record were collected in 8 cm^3 plastic cubes from the working half of cores 738B-3H to 12H (16.52–103.46 m below seafloor (mbsf)) at an average spacing of 60 cm [*Roberts et al*., 2011a]. For the studied interval, the lithology consists of predominantly homogeneous calcareous nannofossil ooze. The average sedimentation rate through the late Eocene portion of the record was ca. 0.8 cm/kyr [*Roberts et al*., 2011a]. Pelagic carbonate samples were selected through the Paleocene-Eocene thermal maximum (PETM) interval from ODP Hole 738C [*Larrasoaña et al*., 2012; *Chang et al*., 2012a] and through the Eocene-Oligocene portion of ODP Holes 689D and 690C [*Florindo and Roberts*, 2005]. Hole 738C was cored on the SKP, which was close to the Antarctic margin during the PETM. The PETM section at this hole comprises a white to light greenish gray calcareous foraminiferal nannofossil chalk with some evidence of bioturbation [*Larrasoaña et al*., 2012]. ODP Holes 689D (64°31.01′S, 3°06.00′E; 2080 m water depth; Eocene-Oligocene paleo water depth 1600 m) and 690C (65°09.62′S, 1°12.29′E; 2914 m water depth; Eocene-Oligocene paleo water depth 2400 m) were cored at Maud Rise, Weddell Sea, Southern Ocean (Figure 1) and represent key calibration points for Southern Ocean Paleogene and Neogene biostratigraphic zonations. The lithologies are marked by foraminifer-bearing, calcareous nannofossil ooze and chalk. Average sedimentation rates through the Eocene-Oligocene at ODP sites 689 and 690 were of the order of 0.6–1 cm/kyr [*Florindo and Roberts*, 2005].

[5] Transmission electron microscope (TEM) observations (e.g., Figures 2a and 2b), and rock magnetic (e.g.,

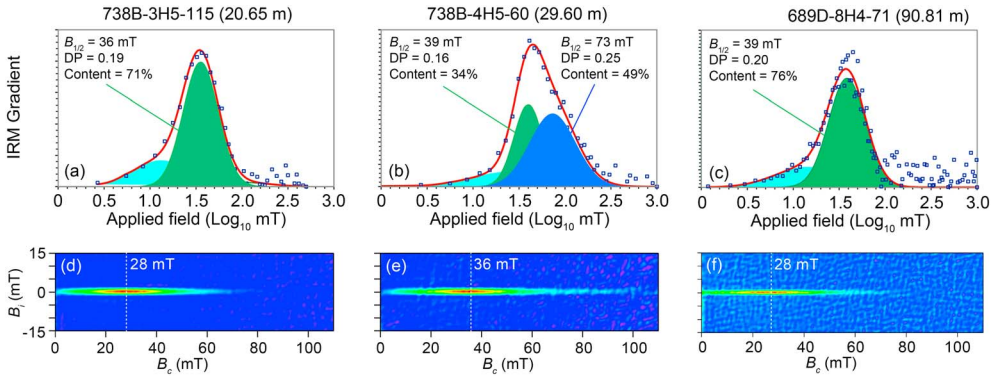

Figure 3. (a–c) IRM components and (d–f) FORC diagrams for selected pelagic carbonates from ODP Holes 738B and 689D. In Figures 3a–3c, squares represent experimental data. Colored areas indicate different IRM components. Red lines are the overall fit from all components. IRM parameters for two components with small DP values (biogenic components) are indicated. In Figures 3d–3f, FORC diagrams were calculated using a smoothing factor of 3. Dotted lines represent the positions of the coercivity peaks of FORC distributions.

Figure 3), including ferromagnetic resonance (FMR), measurements on samples from ODP Sites 738, 689, and 690 indicate that biogenic magnetite dominates their magnetic properties [*Roberts et al*., 2011a, 2012; *Larrasoaña et al*., 2012; *Chang et al*., 2012a]. Samples containing whole MTB cells, including wild-type *Magnetospirillum magneticum* AMB-1 (Figure 2c) [*Kopp et al*., 2006a], uncultivated giant rod-shaped bacterium MYR-1 (Figure 2d) [*Li et al*., 2010] and cultured *Magnetospirillum gryphiswaldense* MSR-1 (Figure 2e) [*Schüler and Köhler*, 1992; *Fischer et al*., 2008; *Scheffel et al*., 2008], and inorganic magnetite and greigite (Fe_3S_4) samples were compared with results from marine carbonates. Inorganic magnetite powders include oxidized synthetic magnetite (ca 50 nm grain size; *Maher* [1988]) and near-stoichiometric magnetite obtained by reducing the oxidized magnetite under a $CO:CO_2$ atmosphere (1:4 ratio) at 230°C for 24 h. The inorganic greigite includes a synthetic pseudo-single-domain (PSD)/multi-domain (MD) sample and a typical natural SD greigite sample previously analyzed by *Chang et al*. [2007, 2008, 2009].

[6] Room-temperature isothermal remanent magnetization (IRM) acquisition and first-order reversal curve (FORC) measurements were made with a Princeton Measurements Corporation MicroMag vibrating sample magnetometer (VSM). FORC measurements [*Pike et al*., 1999; *Roberts et al*., 2000] were made with maximum applied fields of 1 T, field increments up to 0.4 mT, and averaging time of 250 ms. FORC diagrams were calculated using the FORCinel package [*Harrison and Feinberg*, 2008]. A smoothing factor (SF) of 3 [*Roberts et al*., 2000] was used. IRM acquisition curves were obtained by measuring 100–150 field steps (nonlinearly spaced) up to a maximum applied field of 1 T. IRM acquisition curves were decomposed into log-normally distributed coercivity components using the fitting protocol of *Kruiver et al*. [2001]. Low-temperature magnetic measurements of marine carbonates were made at the Center for Advanced Marine Core Research, Kochi University, Japan, using a Magnetic Properties Measurement System (Quantum Design, MPMS-XL5). Measurements on whole MTB cells and inorganic magnetite were carried out at Bremen University, Germany, and Lancaster University, UK, respectively, both using a MPMS-XL7. For zero-field cooled (ZFC) and field-cooled (FC) measurements of a saturation IRM (SIRM) during warming, samples were cooled to 10 K in either zero field or a 2.5 T field, respectively. At 10 K, a 2.5 T field was applied and then switched off to impart a low-temperature SIRM. SIRM warming curves were measured during warming in zero field (the residual field after a magnet reset from 2.5 T is ~200–300 μT). The ZFC warming curves were acquired before the FC curves. For low-temperature cycling (LTC) of a room-temperature SIRM (RTSIRM), remanence was measured from room temperature to 10 K and back to room temperature in zero field. For low-temperature alternating current (AC) susceptibility measurements, samples were cooled in zero field to 10 K and were then measured at several frequencies (1, 10, 100, and 997 Hz) up to 300 K.

3. Results

3.1. Room Temperature Magnetic Properties

[7] Room temperature measurements indicate two main types of magnetic properties for pelagic carbonates from ODP Hole 738B (Figure 3). One type of sample (sample "738B-3H5-115") has a major IRM component with $B_{1/2}$ of ~36 mT and a small DP of 0.19 (green; Figure 3a). A much smaller IRM component at low field (light blue; Figure 3a) is also fitted. We do not interpret this component as a separate magnetic constituent, but rather as an artifact of the *Kruiver et al*. [2001] fitting protocol, which restricts model distributions to be symmetric on a log-scale. This small low-field IRM component is most likely to reflect deviations of the major IRM component from the ideal log-normal model distribution [*Egli*, 2004a, 2004b]. This "skewed-to-the-left" behavior requires an extra component if fitting is restricted to symmetric distributions. A FORC diagram [*Pike et al*., 1999] for this type of sample has a "central ridge" with negligible vertical spread [*Egli et al*., 2010] (Figure 3d). FMR spectra have two low-field peaks, a pronounced high-field peak, and FMR parameters $g_{eff} < 2.0$, $A < 1$, and $\alpha < 0.3$ [*Roberts et al*.,

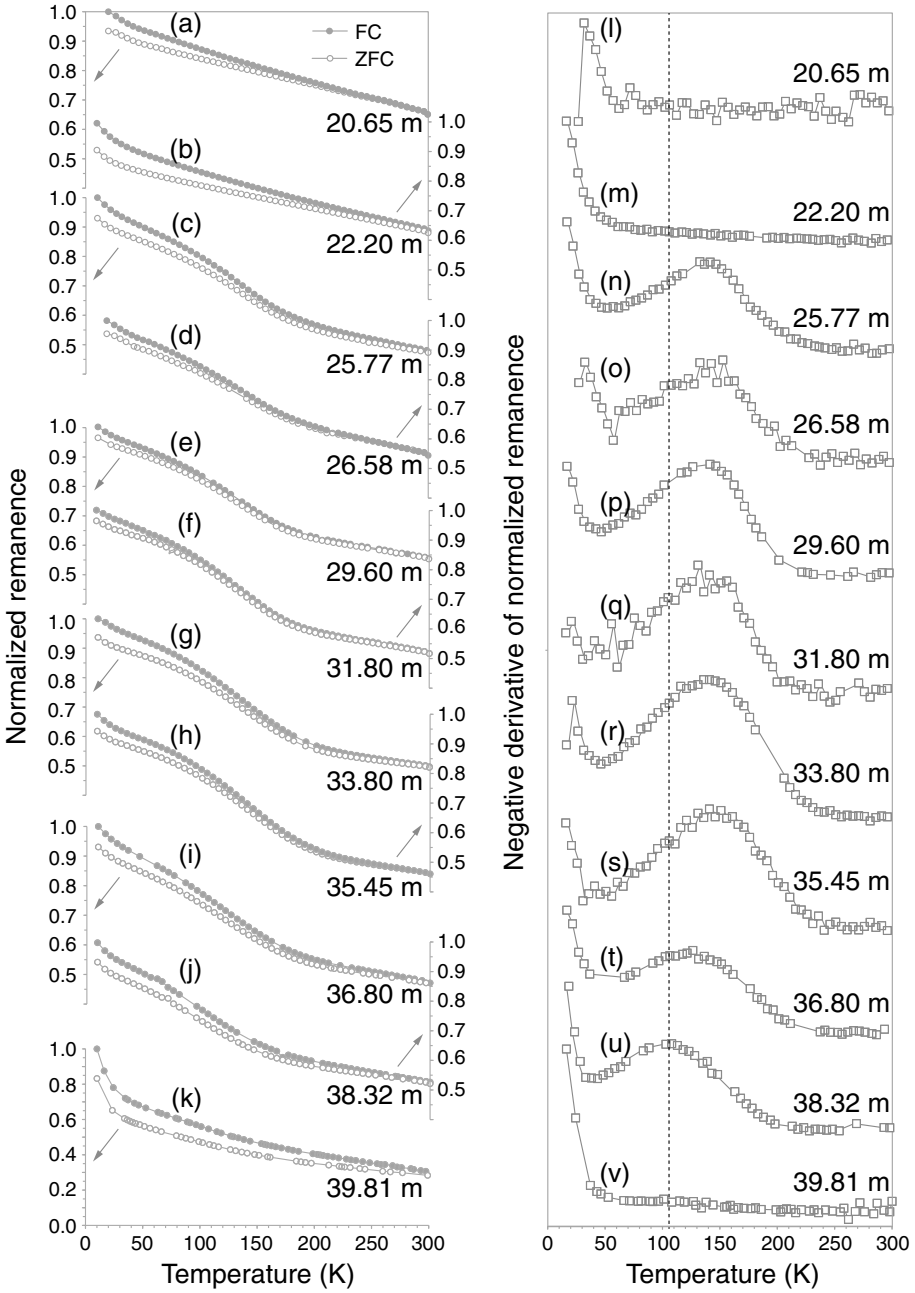

Figure 4. (a–k) Low-temperature warming of SIRM in zero field after ZFC and FC treatments for selected samples from ODP Hole 738B. All data were normalized to the initial SIRM value at low temperatures for the FC curves. (l–v) Corresponding derivatives of the FC curves. Sample positions are indicated as down-core depths. The dotted vertical line indicates the possible T_v (at ~105 K) for partially oxidized biogenic magnetite. Arrows in the left-hand plots indicate the *y* axis of ZFC/FC curves for each sample.

2011a]. All of these results indicate a dominant magnetic signal due to biogenic magnetite, which is consistent with TEM observations (Figures 2a and 2b) [*Roberts et al*., 2011a]. The other type of sample has two major IRM components: one with similar parameters ($B_{1/2}$ and DP values) as those in Figure 3a and the other with a higher $B_{1/2}$ value and also a small DP (0.20–0.25) (blue; Figure 3b). A FORC diagram for this sample has a dominant central ridge, with the peak coercivity shifted to higher values and a longer tail of the central ridge (Figure 3e). It has been suggested that distinct coercivity spectra of biogenic magnetite samples are due to morphological differences: a biogenic soft (BS) component corresponds to equant crystals, and a biogenic hard (BH) component corresponds to elongated crystals [*Egli*, 2004a, 2004b]. For biogenic magnetite, stronger shape anisotropy should increase the coercivity. FMR spectra have similar shapes for the studied samples [*Roberts et al*., 2011a], but the asymmetry ratio *A* has much reduced values (with a lowest value of 0.6) for samples with higher coercivities. FMR theory and experimental observations demonstrate that reduced *A* values — an indication of more asymmetric spectra —

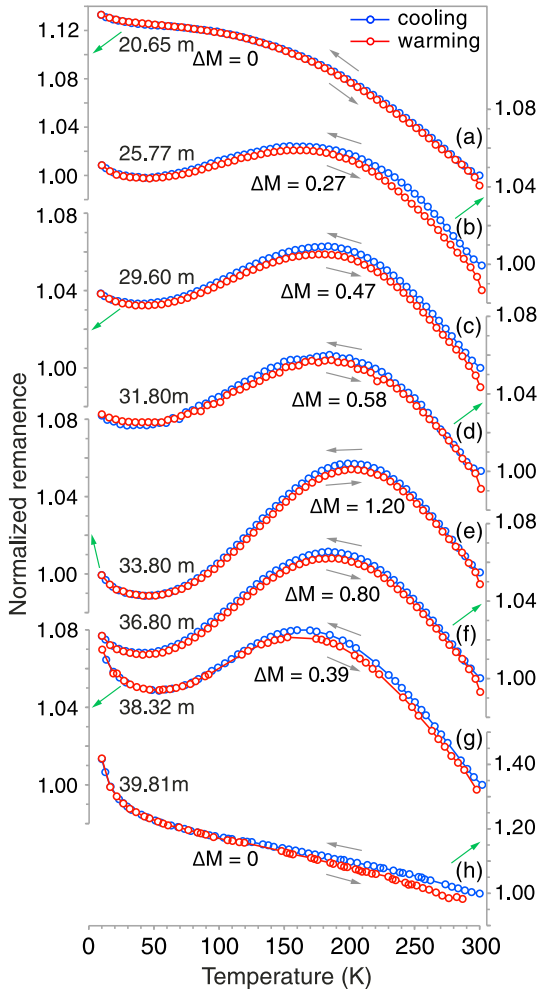

Figure 5. Low-temperature cycling of a RTSIRM in zero field for selected samples from ODP Hole 738B. Arrows indicate the directions of cooling and warming. Blue and red circles represent cooling and warming data, respectively. Green arrows indicate the *y* axis of the LTC cooling-warming curves for each sample. Δ*M* values (as defined in Figure 8) are indicated for each LTC curve.

are caused by increasing shape anisotropy due to either chain arrangement and/or particle elongation [e.g., *Weiss et al.*, 2004; *Kopp et al.*, 2006a, 2006b; *Charilaou et al.*, 2011; *Chang et al.*, 2012b]. Our rock magnetic and FMR measurements therefore indicate the presence of both BS and BH components in some samples. Most of the studied samples from ODP Holes 689D and 690C, however, appear to contain a predominant BS component (Figures 3c and 3f), similar to those presented in Figures 3a and 3d.

3.2. Low-Temperature Magnetic Properties

3.2.1. Low-Temperature SIRM Warming

[8] Results of low-temperature SIRM warming experiments after ZFC and FC treatments [*Moskowitz et al.*, 1993] for carbonates from ODP Hole 738B are presented in Figure 4. Samples from the upper section, i.e., at 20.65 and 22.20 mbsf, have a continuous remanence decay during warming to room temperature (Figures 4a and 4b). The Verwey transition is not apparent in derivatives of the FC curves (Figures 4l and 4m), which is probably due to partial magnetite oxidation. The FC curves have stronger magnetizations than the ZFC curves, but the difference is relatively small (Figures 4a and 4b). Absence of a Verwey transition indicates that biogenic magnetite has been mostly oxidized to maghemite (γ-Fe_2O_3). Samples from the lower part of the studied section, i.e., down to 38.32 mbsf, have enigmatic low-temperature SIRM warming curves with a relatively large remanence drop (Figures 4c–4j). Derivatives of the FC curves contain a broad peak (mostly at ~140 K) (Figures 4n–4s), which is well above T_v for both nonstoichiometric and stoichiometric magnetite (120–125 K) [e.g., *Muxworthy and McClelland*, 2000; *Walz*, 2002]. For some samples (e.g., 36.80 and 38.32 mbsf), this broad peak occurs at lower temperatures of ~120 K and ~105 K (Figures 4t and 4u), respectively. Another characteristic of this type of ZFC/FC curves is that remanence changes are much more gradual, unlike those often observed across T_v where magnetic properties change sharply. We did not observe a clear and sharp discontinuity around T_v, although some samples have a weak peak in the derivative curves at ~105 K. The ZFC and FC curves for these samples do not overlap, with the FC curves slightly higher than the ZFC curves. The remanence loss for most samples is large (~45–55% for FC curves between 10 and 300 K). Samples from the lower part of the studied section undergo continuous remanence loss during warming without any clear peak (Figures 4k and 4v). A large remanence drop, particularly below 40 K, is observed for the sample from 39.81 mbsf.

3.2.2. Low-Temperature Cycling of RTSIRM

[9] LTC cooling and warming curves of a RTSIRM for the upper part of the studied interval of ODP Hole 738B (Figure 5; 20.65 mbsf) undergo a progressive increase during cooling, with a gradual decrease when warming back to room temperature. Cooling and warming curves are almost reversible, resulting in almost no remanence loss during LTC (<1%, Figure 5a). The remanence increase during cooling is about 13% between room temperature and 10 K. Such cooling and warming curves are consistent with the properties of SD maghemite [*Özdemir and Dunlop*, 2010], which indicates that SD biogenic magnetite in this sample is mostly oxidized to maghemite. Samples from the lower part of the studied interval have different LTC behavior (Figures 5b–5g) compared to the uppermost studied sample (Figure 5a). For cooling curves, the remanence first increases with decreasing temperature then decreases to a local minimum (mostly between 40 and 45 K), with a further small increase when cooling to 10 K. The warming curves nearly mimic the cooling curves, which are almost reversible (~1% remanence loss) during LTC. The hump-like shape of cooling curves resembles those for partially oxidized synthetic magnetite [*Özdemir and Dunlop*, 2010]. The peak temperature of the hump for cooling and warming curves varies between ~150 and 200 K (Figures 5b–5g). The shape of the hump-like curves also varies with an apparently continuous change through the studied portion of ODP Hole 738B (Figures 5b–5g).

3.2.3. Low-Temperature AC Susceptibility

[10] Temperature-dependence of in-phase susceptibility (χ') at multiple frequencies (Figure 6) decreases significantly for all samples when warming from the lowest measured

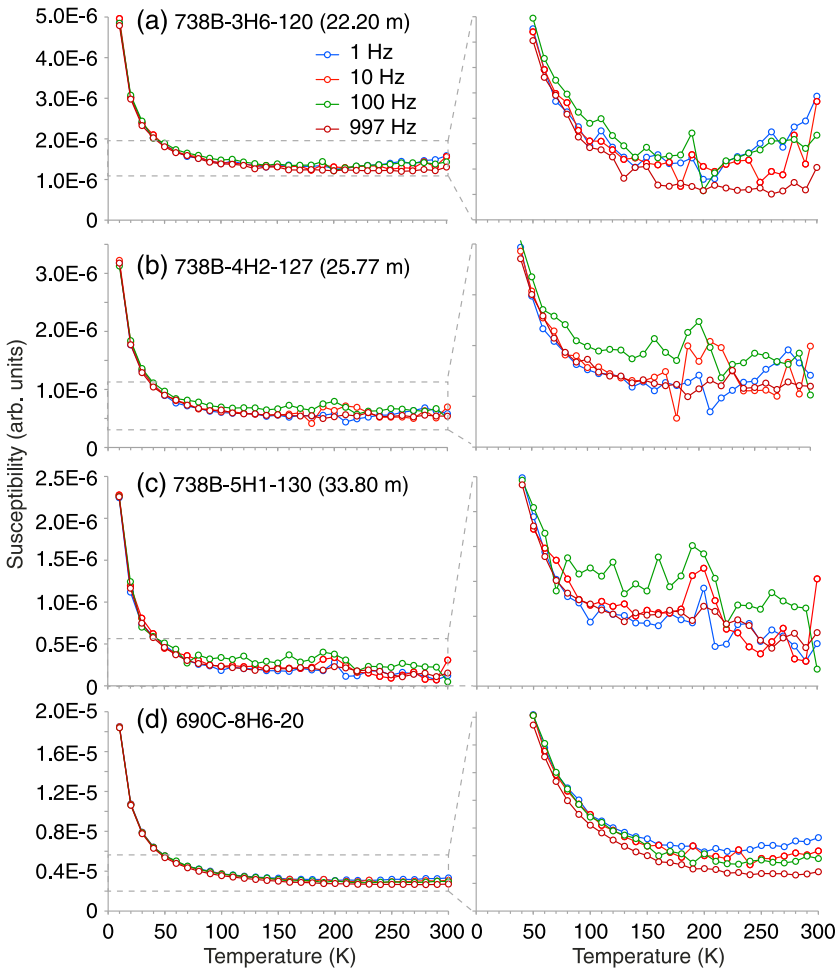

Figure 6. Low-temperature in-phase AC susceptibility measured with different frequencies (1, 10, 100, and 977 Hz) for selected marine carbonates from ODP Holes 738B and 690C. Enlargements of the dashed areas are shown on the right-hand side of the figure.

temperatures. This is mainly attributed to the presence of paramagnetic materials (probably manganese-bearing minerals and iron-bearing silicates), where paramagnetic susceptibility depends inversely on temperature and has no frequency dependence. All measured samples have nearly negligible frequency dependence at low temperatures (i.e., < 50 K; Figure 6), especially when considering measurement noise in these weakly magnetic samples. This indicates that the constituent SD particles are fully blocked thermally at the lowest temperatures. As temperature increases, susceptibility gradually diverges at different frequencies. This indicates that some SD particles become gradually unblocked and exhibit SP behavior with increasing temperature. Out-of-phase susceptibility (χ") results (data not shown) for the measured carbonates are generally even noisier, except for sample "690C-8H6-20" where χ" progressively increases with increasing temperature, which is consistent with SP behavior. The SP behavior can have several origins, for example, from the presence of small immature magnetosome crystals, fractions of ultrafine oxidized/unoxidized magnetite that occur below the SP/SD threshold size for magnetite, and ultrafine magnetic particles produced by reductive diagenesis in pelagic environments [*Tarduno*, 1995; *Smirnov and Tarduno*, 2000]. For some samples ("738B-3H6-120" and "690C-8H6-20"), the AC susceptibility curves have a simple shape, with gradual divergence of susceptibility depending on frequency (generally higher susceptibility at lower frequency) (Figures 6a and 6d). Samples from the enigmatic interval of ODP Hole 738B have relatively complex and nonmonotonic behavior. The noticeable changes between ~100 and 200 K (Figures 6b and 6c) may reflect SP behavior. However, the noisy data for these samples preclude definite interpretation.

4. Discussion

4.1. Low-Temperature Magnetism of Pelagic Carbonates: Magnetite Oxidation

[11] In order to compare systematically the magnetic properties of the studied samples from ODP Hole 738B (Figures 4–6), we summarize a range of typical low-temperature magnetic results for representative pelagic carbonates and samples containing whole MTB cells (Figure 7). We interpret the main differences between the low-temperature ZFC/FC SIRM warming curves (Figures 7a–7g) and LTC of RTSIRM curves (Figures 7h–7n) to be due to different degrees of magnetite oxidation (maghemitization) (Figure 7o) [see also *Smirnov and Tarduno*, 2000]. It has

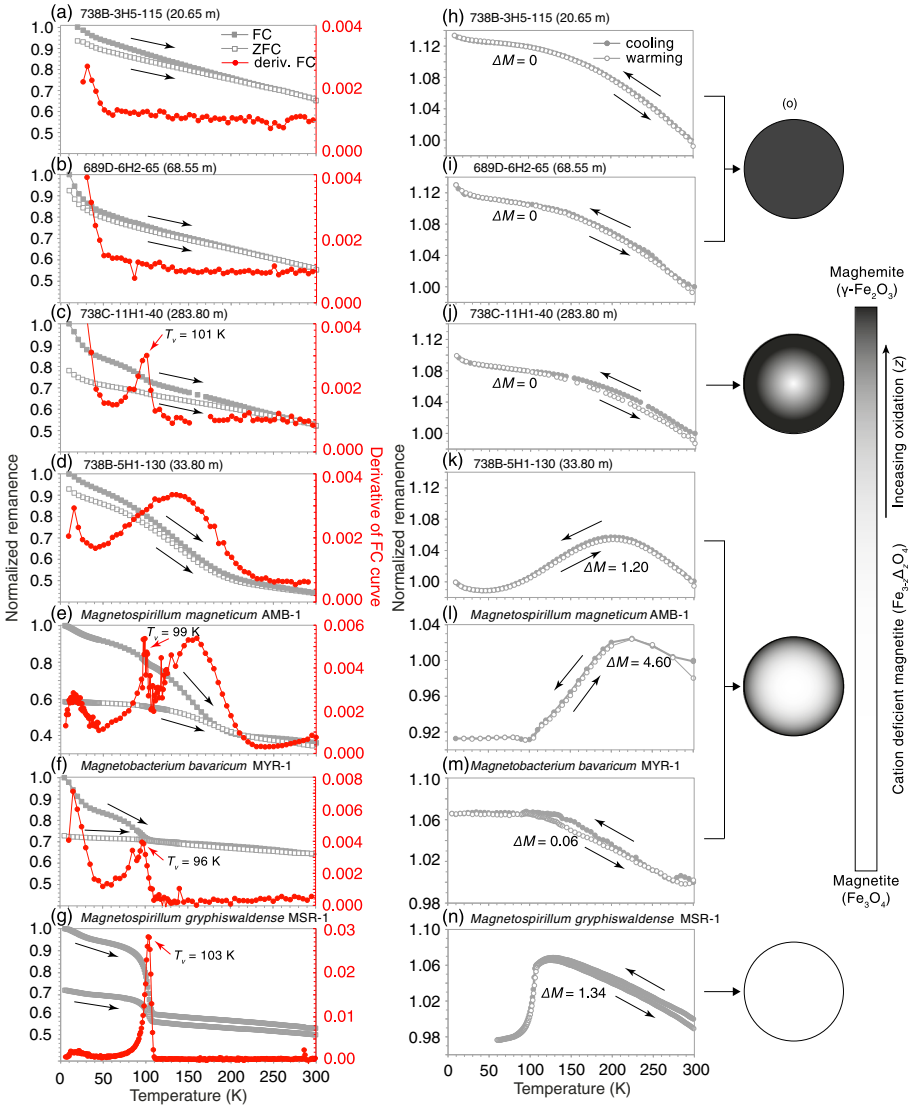

Figure 7. Systematic presentation of low-temperature magnetic properties for samples containing biogenic magnetite (marine carbonates and whole MTB cells). (a–g) Low-temperature SIRM warming in zero field after ZFC/FC treatments. (h–n) Low-temperature cycling of RTSIRM in zero field. Marine carbonates are from ODP Holes 738B, 738C, and 689D. Samples that contain whole MTB cells with biogenic magnetite chains include (e, l) wild-type *Magnetospirillum magneticum* AMB-1 [*Kopp et al.*, 2006a], (f, m) uncultivated giant rod-shaped bacterium MYR-1 [*Li et al.*, 2010], and (g, n) cultured *Magnetospirillum gryphiswaldense* MSR-1 [*Schüler and Köhler*, 1992; *Scheffel et al.*, 2008]. The low-temperature properties can be divided into four main groups depending on the degree of oxidation: fully oxidized, highly oxidized, moderately or slightly oxidized, and nearly fresh biogenic magnetite within whole MTB cells. Images on the right are illustrations of biogenic magnetite crystals with different degrees of oxidation. The oxidation degree could decrease continuously from the surface to the magnetite core, with no sharp boundary between stoichiometric magnetite and partially oxidized magnetite. ΔM values are indicated for each LTC curve.

also been demonstrated that biogenic magnetite crystals have various oxidation degrees, using TEM observations [*Vali et al.*, 1987] and high-resolution synchrotron X-ray diffraction [*Fischer et al.*, 2011]. Therefore, we categorize typical low-temperature magnetic results according to the degree of biogenic magnetite oxidation: (a) fully oxidized, (b) highly oxidized, (c) moderately to slightly oxidized, and (d) negligibly oxidized (fresh magnetite). Below, we describe the general low-temperature magnetic behavior for each group and present physical mechanisms to explain the observed properties. Here we only provide general mechanisms; exact physical explanations need further investigation.

4.1.1. Fully Oxidized Biogenic Magnetite

[12] For biogenic magnetite that has been fully oxidized to maghemite, low-temperature ZFC/FC SIRM warming curves undergo a monotonic decrease without a Verwey transition (Figures 7a and 7b). This type of SIRM warming curve has been commonly observed for natural samples containing

biogenic magnetite [e.g., *Yamazaki and Ioka*, 1997; *Smirnov and Tarduno*, 2000; *Weiss et al*., 2004; *Yamazaki and Solheid*, 2011; *Roberts et al*., 2012]. LTC RTSIRM curves have a gradual remanence increase during cooling and a reversible warming curve with respect to the cooling curve (Figures 7h and 7i). Such LTC curves have been observed for oxidized magnetite [e.g., *van Velzen and Zijderveld*, 1990; *Passier and Dekkers*, 2002], and are consistent with the behavior of SD maghemite [*Özdemir and Dunlop*, 2010]. This end-member, unsurprisingly, has relatively simple low-temperature magnetic properties. First, fully oxidized magnetite has no Verwey transition and therefore has no sharp change in magnetic properties across T_v, unlike magnetite [e.g., *Muxworthy and McClelland*, 2000]. Second, SD particles should have a monotonic temperature dependence, which mainly reflects the temperature dependence of the spontaneous magnetization [*Özdemir and Dunlop*, 2010]. In contrast, magnetic mineral assemblages with significant concentrations of SP particles and PSD/MD grains should undergo magnetic unblocking at low temperatures during SIRM warming, and irreversible low-temperature demagnetization behavior due to domain wall dynamics [e.g., *Moskowitz et al*., 1998; *Muxworthy et al*., 2003; *Chang et al*., 2009], respectively. We see no evidence of low-temperature magnetic behavior expected for PSD/MD grains. The relatively larger SP concentration, as evident in the remanence drop (~30–40%) during SIRM warming and in the temperature-dependent AC susceptibility, should not make contributions to the LTC experiments. This supports our interpretation that the monotonic remanence curves are due to SD maghemite. Low-temperature magnetic behavior for fully oxidized biogenic magnetite is commonly observed in pelagic carbonates probably due to magnetite oxidation during long-term geological burial and/or to postsampling storage [e.g., *Smirnov and Tarduno*, 2000].

4.1.2. Highly Oxidized Biogenic Magnetite

[13] For highly oxidized biogenic magnetite, low-temperature SIRM warming curves, particularly FC curves, can still contain evidence of a well-defined T_v. This T_v (Figure 7c) often occurs at slightly lower temperature (mostly ~100 K) in biogenic magnetite [e.g., *Pan et al*., 2005b] than for stoichiometric inorganic magnetite [*Walz*, 2002]. Expression of the T_v is subdued and suppressed in partially oxidized magnetite [*Özdemir et al*., 1993; *Cui et al*., 1994; *Özdemir and Dunlop*, 2010]. The slightly reduced T_v below 120 K may indicate that a small core of the biogenic magnetite crystals still has a composition close to that of magnetite, while a thick shell has been oxidized to maghemite. Highly oxidized biogenic magnetite usually has a large difference between FC and ZFC curves, particularly below 40–50 K (Figure 7c). The detectable Verwey transition probably indicates that the core of the biogenic magnetite crystals still consists of fresh stoichiometric magnetite, although a significant fraction of the outer surfaces has been oxidized to maghemite [e.g., *Cui et al*., 1994; *Torii*, 1997; *Smirnov and Tarduno*, 2000; *Özdemir and Dunlop*, 2010] (Figure 7o). This type of ZFC/FC SIRM warming curve is widely observed for marine carbonates [e.g., *Smirnov and Tarduno*, 2000; *Weiss et al*., 2004; *Yamazaki and Solheid*, 2011; *Roberts et al*., 2012]. For LTC of a RTSIRM, both cooling and warming curves undergo a largely monotonic change. The Verwey transition is nearly smeared-out, although minor divergence occurs between the Verwey transition and room temperature (Figure 7j). Changes in remanence during cooling (~10%; Figure 7j) are slightly smaller compared to those for fully oxidized samples (~13%; Figures 7h and 7i). The remanence loss during LTC is still small (~2%). This type of LTC curve has been observed for pelagic sediments [e.g., *Yamazaki*, 2009]. Significantly oxidized biogenic magnetite, therefore, has similar low-temperature magnetic properties to fully oxidized magnetite, which makes it difficult to fully distinguish them. However, highly oxidized biogenic magnetite may still have a weak but detectable T_v. Regardless, it is likely that highly oxidized biogenic magnetite, even with a detectable T_v, will fail the low-temperature ZFC/FC test of *Moskowitz et al*. [1993].

4.1.3. Moderately to Slightly Oxidized Biogenic Magnetite

[14] For moderately to slightly oxidized biogenic magnetite, we observed enigmatic low-temperature magnetic properties in both SIRM warming (Figures 7d–7f) and LTC curves (Figures 7k–7m). Low-temperature SIRM warming curves have broad remanence drops that have not been commonly observed for magnetite. *Smirnov and Tarduno* [2000] observed broad ZFC/FC curves without a detectable T_v for a pelagic carbonate sample from ODP Site 851. The peak temperature for the remanence drop in their sample appears to be higher compared to our measured samples from ODP Site 738B. *Özdemir and Dunlop* [2010] observed a broad remanence drop between ~10 and 40 K in SIRM warming curves for slightly oxidized magnetite. This initial remanence drop almost disappeared when their sample was reduced to stoichiometric magnetite. The low unblocking temperatures imply a particle size of only ~10 nm, which *Özdemir and Dunlop* [2010] attributed to a thin maghemite surface shell. The large and broad SIRM drops in our samples (peaks mostly at ~100–140 K) are also likely to be associated with magnetite oxidation. The higher unblocking temperature for our observed remanence drop (Figures 4 and 7d) compared to those of *Özdemir and Dunlop* [2010] indicate slightly larger SP sizes in our samples. This suggests a greater degree of oxidation, which probably has also further suppressed the Verwey transition. The broad peak temperature range also spans T_v, which is probably why we do not observe a clear Verwey transition temperature. Derivative data indicate a weak inflection at around 105 K for some samples (Figures 4n–4u), which probably corresponds to a Verwey transition signature. This large SP fraction may have resulted from partial oxidation of biogenic magnetite, and/or from the ultrafine magnetic particles surrounding biogenic magnetite particles produced during reductive diagenesis in pelagic environments, as described by *Tarduno* [1995] and *Smirnov and Tarduno* [2000].

[15] ZFC/FC curves for a sample containing wild-type *Magnetospirillum magneticum* AMB-1 cells also have broad remanence drops but with a large divergence between the ZFC and FC curves (Figure 7e) [*Kopp et al*., 2006a]. The derivative of the FC curve indicates a sharp peak at ~100 K, and two broad peaks at ~15 and 210 K, respectively. The sharp peak at 100 K reflects T_v, while the broad peaks are interpreted to reflect oxidation of biogenic magnetite. In contrast, the sharp remanence drop at the Verwey transition and lack of a broad drop above T_v indicates that biogenic magnetites within other studied AMB-1 samples [e.g., *Weiss et al*., 2004; *Prozorov et al*., 2007; *Li et al*., 2009]

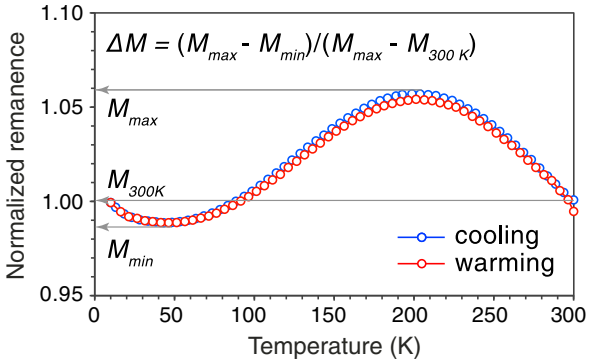

Figure 8. Definition of the parameter ΔM that describes the relative change of LTC RTSIRM curves to indicate the degree of oxidation. $\Delta M = (M_{max} - M_{min})/(M_{max} - M_{300\ K})$, where M_{max}, M_{min}, and $M_{300\ K}$ represent the maximum, minimum, and the initial remanence at 300 K, respectively. The measured data are from a typical marine carbonate sample from ODP Hole 738B (33.80 mbsf), which has the highest ΔM value and the most significant hump-like curve.

are fresher compared to that studied by *Kopp et al*. [2006a]. These results support the interpretation that the SIRM warming curves with broad remanence drops are caused by oxidation of biogenic magnetite. ZFC/FC SIRM warming curves for an uncultivated giant rod-shaped MYR-1 sample [*Li et al*., 2010] (Figure 7f) contain distinct warming behavior across T_v with a relatively large divergence between ZFC and FC curves below T_v (Figure 7f).

[16] For LTC of RTSIRM for moderately to slightly oxidized magnetite, cooling curves first increase and then decrease to a local minimum before recovering slightly at the lowest measured temperatures (Figures 5b–5g and 7k). Warming curves are nearly reversible with respect to cooling curves. LTC cooling curves that first increase and then decrease before approaching T_v have been observed for partially oxidized synthetic magnetite [*Özdemir and Dunlop*, 2010], and for sediment samples [e.g., *Yamazaki et al*., 2003; *Yamazaki and Solheid*, 2011; *Yamazaki and Ikehara*, 2012]. Humped reversible cooling-warming curves have not been reported for natural samples. LTC cooling-warming curves for wild-type *Magnetospirillum magneticum* AMB-1 with hump-like reversible curves (Figure 7l) [*Kopp et al*., 2006a] are similar to those for our ODP 738B samples (Figures 5b–5g), except with a well-defined T_v at ~100 K (Figure 7l). Considering that this AMB-1 sample has similar SIRM warming curves to the ODP 738B samples, our results indicate that similar oxidation has affected these samples. For the uncultivated MYR-1 sample, the LTC cooling curve first increases to ~130 K. The remanence then remains almost constant during cooling to 10 K (Figure 7m) [*Li et al*., 2010]. The warming curve is almost reversible with respect to the cooling curve until ~100 K, at which point the remanence decreases from 100 K to 300 K. There is nearly no remanence loss although the cooling and warming curves are not completely reversible around T_v (Figure 7m).

[17] To describe the hump-like LTC curves, we propose a parameter $\Delta M = (M_{max} - M_{min})/(M_{max} - M_{300\ K})$ (defined in Figure 8), where M_{max}, M_{min}, and $M_{300\ K}$ represent the maximum, minimum, and the initial remanence at 300 K, respectively. ΔM can be used as an indication of different oxidation degrees in biogenic magnetite. For example, larger ΔM values correspond to a large remanence decrease during cooling and therefore indicate a lower oxidation degree. Samples from the studied interval within ODP Hole 738B undergo a continuous change in ΔM, with the highest value at 33.80 mbsf (Figures 5 and 7k), which corresponds to the lowest degree of oxidation according to this scheme. Fully or highly oxidized biogenic magnetite samples do not exhibit humped LTC curves, for which we therefore set the ΔM value to zero. It should be noted that ΔM can only reflect relative oxidation degree. It is different from the parameters ΔM_c (for the cubic phase above T_v) and ΔM_m (for the monoclinic phase below T_v) defined by *Özdemir and Dunlop* [2010], which we did not use because, in contrast to their data, LTC curves for our samples are almost reversible.

[18] The observed hump-like LTC curves are caused by partial magnetite oxidation; however, we lack a detailed mechanism to explain the smooth hump shape. *Özdemir and Dunlop* [2010] suggested that the shape and magnitude of the hump in LTC cooling curves could be predicted roughly by a simple model with linear combinations of fresh magnetite and maghemite. Most other observed low-temperature magnetic behavior of oxidized magnetite, such as the much-reduced T_v, and the humped warming curves, are difficult to predict with their simple model. This indicates that some other mechanism must also be involved, such as complex magnetic interactions or exchange coupling at the magnetite-maghemite interface, and/or a continuous decrease in oxidation degree from the surface to the core of a magnetite particle (Figure 7o).

4.1.4. Fresh Biogenic Magnetite Within Intact MTB Cells

[19] We measured the low-temperature properties of a sample of the cultured MTB strain *Magnetospirillum gryphiswaldense* MSR-1 [*Schüler and Köhler*, 1992; *Scheffel et al*., 2008] that contains fresh biogenic magnetite (Figure 2e). ZFC/FC SIRM warming curves for this sample contain distinct warming behavior across the Verwey transition with a large divergence between the ZFC and FC curves below T_v (Figure 7g), as indicated by an extremely sharp T_v in the derivative of the FC curve at 103 K. This behavior is an indication of the presence of magnetosome chains consisting of fresh magnetite [e.g., *Moskowitz et al*., 1993; *Carter-Stiglitz et al*., 2002, 2004; *Weiss et al*., 2004; *Pan et al*., 2005a, 2005b; *Li et al*., 2009, 2010, 2012]. In LTC cooling-warming curves, the remanence first increases during cooling and peaks at ~130 K, the isotropic point for magnetite [*Bickford et al*., 1957]. The remanence then decreases gradually to ~107 K, below which an extremely large remanence drop occurs (Figure 7n). This large drop is due to the Verwey transition. The warming curve is almost reversible with respect to the cooling curve (Figure 7n), with only a small remanence loss during LTC treatment (~1%). Published LTC curves for samples with whole MTB cells are often nearly reversible during cooling and warming, with well-defined low-temperature transitions either at T_v or at the isotropic point [e.g., *Carter-Stiglitz et al*., 2004; *Kopp et al*., 2006a, 2006b]. *Carter-Stiglitz et al*. [2004] reported a large remanence drop of ~12% on cooling across T_v for a fresh sample containing whole cells from MTB strain MV1, but a much reduced remanence drop of only ~1% for an "aged" MV1 sample. This remanence drop for our fresh MSR-1

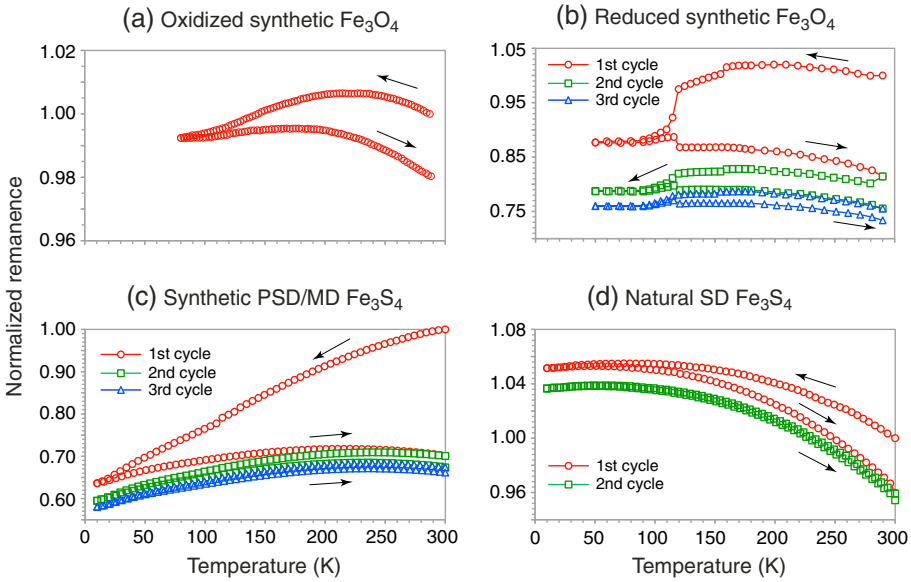

Figure 9. Consecutive cooling-warming cycles for a RTSIRM (red circles: first cycle, green squares: second cycle, blue triangles: third cycle) for inorganic magnetic minerals: (a) synthetic magnetite after reduction for 24 h under a $CO:CO_2$ atmosphere (1:4 ratio) at 230°C, (b) synthetic magnetite after reduction for 30 h under a $CO:CO_2$ atmosphere (1:4 ratio) at 230°C, (c) a synthetic greigite with dominant PSD/MD grains, and (d) natural greigite from Italy with dominant SD grains.

sample is ~10% (Figure 7n), which is close to that of the fresh MV1 sample [*Carter-Stiglitz et al.*, 2004]. As discussed earlier, some of our marine carbonate samples with less oxidized biogenic magnetite also have reversible LTC curves, but without clear transitions near T_v or at the isotropic point for magnetite. Details about the humped reversible cooling-warming LTC curves and associated mechanisms are discussed below. Marine carbonates with similar magnetic properties to fresh biogenic magnetite are rare. This is not surprising because fine-grained magnetite is likely to oxidize (to various degrees) during prolonged geological burial or during sample storage [*Peck and King*, 1996]. This is probably why natural magnetosome-bearing samples with low-temperature properties close to those of fresh biogenic magnetite have been mostly reported from surface sediments [e.g., *Pan et al.*, 2005b; *Kim et al.*, 2005; *Housen and Moskowitz*, 2005; *Kopp et al.*, 2006b; *Maloof et al.*, 2007] or from the water column [*Moskowitz et al.*, 2008].

4.2. Low-Temperature Magnetism of Nonbiogenic Magnetite and Greigite

[20] As discussed above, cooling-warming curves for partially oxidized biogenic samples have variable temperatures for their humps but are still nearly reversible (Figures 5b–5g, 7k, and 7l). In contrast, nonreversible LTC cooling-warming curves (i.e., with remanence loss) are observed for synthetic magnetite powders, for both oxidized (Figure 9a) and stoichiometric magnetite (Figure 9b) [e.g., *Özdemir and Dunlop*, 2010]. For our oxidized synthetic magnetite, both cooling and warming LTC curves have humped shapes, but are not reversible. The peak temperature of the hump of the warming curve is always higher than for the cooling curve (Figure 9a). In contrast, the peak temperature of the hump for our biogenic magnetite samples is identical for cooling and warming curves (Figures 5b–5g). For reduced inorganic magnetite samples (close to stoichiometric magnetite), LTC cooling curves have a broad humped peak above T_v (Figure 9b), and a large remanence drop when cooling through T_v. Below T_v, the warming curves are nearly reversible with respect to cooling curves with a large remanence drop when warming through T_v. Much remanence is therefore lost during LTC. *Muxworthy and Williams* [2006] micromagnetically simulated LTC curves for stoichiometric magnetite with magnetostatic interactions. Their result for a magnetite assemblage with $q = 1.1$ and $d/r = 0.5$ (q is the ratio of the long to the short axis of particles, and d/r is the grain size divided by the grain separation measured from the grain center) is similar to the LTC curve for our nearly stoichiometric magnetite powder samples (Figure 9b). The nature of our inorganic magnetite sample is consistent with the model parameters. Repeated second and third consecutive LTC runs (Figure 9b) have similar behavior as the first cycle, except for a much smaller remanence loss.

[21] For magnetic minerals that lack a low-temperature transition, such as greigite [e.g., *Chang et al.*, 2009; *Roberts et al.*, 2011b] and maghemite [e.g., *Özdemir and Dunlop*, 2010], nonreversible LTC curves are often observed (Figures 9c and 9d). For a synthetic PSD/MD greigite sample [*Chang et al.*, 2007, 2008], the cooling curve during the first cycle has a monotonic remanence decrease. The warming curve is not reversible with respect to the cooling curve, and there is a large remanence loss (Figure 9c) [*Chang et al.*, 2007, 2009]. During the second cycle, the cooling curve also has a remanence decrease, although it is much smaller compared to the first cooling. The warming curve has a large remanence recovery with only a small remanence loss (Figure 9c). Cooling-warming curves for a third LTC run are nearly reversible (Figure 9c). The nonreversible LTC behavior and large remanence loss during the first LTC treatment are probably associated with domain wall

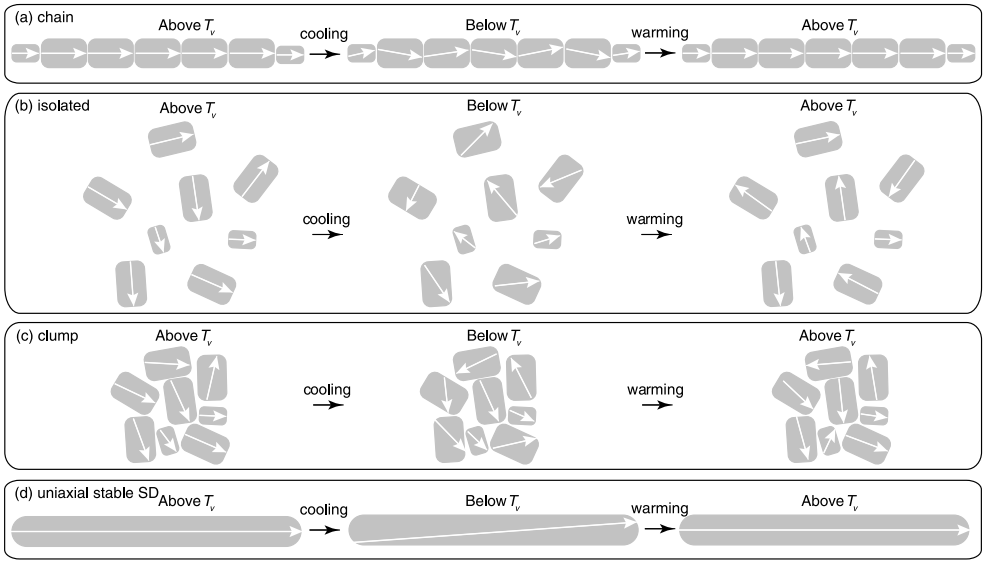

Figure 10. Illustrations of the dipole spring mechanism for (a) intact biogenic magnetite chains and an absence of such a mechanism for assemblages of (b) isolated SD magnetic crystals, and (c) clumped SD magnetic grains. (d) Illustration of an isolated uniaxial stable SD particle to compare with the dipole spring mechanism. The left-hand column represents the saturation remanence state above T_v before cooling. The middle column indicates the magnetic state after cooling below T_v. The right-hand column illustrates the remanent state when warming back above T_v. White arrows indicate directions of the magnetic moments for each magnetic crystal. In Figure 10a, the dipole spring mechanism causes reversible cooling-warming LTC behavior and a restoration of remanence for biogenic magnetite chains. In Figures 10b and 10c, the absence of such a mechanism produces more random distributions of magnetic moments that result in remanence loss and irreversible LTC curves. The case of isolated particles in Figure 10b is appropriate only for randomly oriented particles and does not take into account the controlled alignment model of *Muxworthy and Williams* [2006].

unpinning for PSD/MD magnetic mineral assemblages [e.g., *Moskowitz et al*., 1998; *Muxworthy et al*., 2003; *Chang et al*., 2007, 2009]. For a natural greigite sample with typical SD behavior [*Chang et al*., 2007, 2008, 2009], the cooling curve during the first LTC run has a progressive remanence increase. The warming curve decreases progressively, but is not reversible with respect to the cooling curve (Figure 9d). Therefore, there is a moderate remanence loss (~4%). Cooling-warming curves during the second LTC treatment have almost reversible behavior (remanence loss of only ~0.5%; Figure 9d). The remanence loss during the first cycle is probably associated with small amounts of large PSD/MD greigite crystals within this dominantly SD sample. The presence of PSD/MD greigite grains [*Chang et al*., 2007] is not surprising because, unlike the precise size control of MTB biomineralization, diagenesis does not provide a precise size control over formation of SD greigite. For maghemite, reversible LTC cooling-warming curves were observed for acicular SD particles [e.g., *Özdemir and Dunlop*, 2010]. The reversible LTC curves for acicular maghemite are not due to chain signatures. Maghemite does not have a low-temperature transition, and the measured maghemite sample has SD magnetic properties; therefore, no remanence loss is expected during LTC treatment.

4.3. The Dipole Spring Mechanism: A Diagnostic Indicator of Intact Magnetosome Chains

[22] Despite different shapes of LTC cooling-warming curves, our results, together with published data [*Carter-Stiglitz et al*., 2004; *Kopp et al*., 2006a, 2006b; *Li et al*., 2010, 2013], consistently indicate almost reversible cooling-warming behavior for samples containing both fresh (Figures 7m and 7n) and oxidized (Figures 7h–7l) biogenic magnetite. In contrast, natural inorganic magnetite and synthetic magnetite powders often undergo significant remanence loss during LTC treatment (Figures 9a and 9b; [*Hartstra*, 1982; *Özdemir and Dunlop*, 2010]). Two theoretical studies [*Carter-Stiglitz et al*., 2004; *Muxworthy and Williams*, 2006] predict reversible LTC curves for stoichiometric magnetite, including assemblages with randomly oriented, isolated magnetite crystals and chains with 10 magnetosome crystals [*Carter-Stiglitz et al*., 2004] and magnetite with controlled alignment [*Muxworthy and Williams*, 2006]. The reversible LTC curves are explained by considering the magnetic anisotropy of uniaxial stable SD particles. When cooling across magnetite's T_v phase transition, the magnetic moment of any single uniaxial particle will rotate away from the long axis of the SIRM state. When warming back above T_v, the magnetic moment can rotate back into the original direction [*Carter-Stiglitz et al*., 2004], probably due to "controlled switching" of magnetic moments [*Muxworthy and Williams*, 2006].

[23] Why, then, do samples containing intact magnetosome chains also have reversible LTC behavior, even though there are strong magnetostatic interactions among magnetosome crystals? We explain this observation by invoking a dipole spring mechanism (Figure 10). Dipolar interactions within magnetosome chains [e.g., *Dunin-Borkowski et al*., 1998;

Simpson et al., 2005] produce a strong uniaxial anisotropy [e.g., *Moskowitz et al*., 1993; *Penninga et al*., 1995; *Hanzlik et al*., 2002; *Egli et al*., 2010], which stabilizes the magnetization distributions within magnetosome chains. Stabilizing dipolar interactions act like a spring that provides a restoring force across T_v. Above T_v before cooling, the magnetization of biogenic magnetite chains is controlled by dipole interactions and shape anisotropy. There is no competition between magnetostatic interactions and magnetic anisotropy because the <111> magnetic easy axis is aligned along the chain axis (Figure 10a). The saturation remanent state therefore produces parallel magnetic moments along the chain axis. When cooling below T_v, the cubic magnetite phase transforms into a phase with lower structural symmetry (i.e., monoclinic or triclinic) with the <111> crystallographic direction being no longer the easy axis. Therefore, the magnetic moment would not be as strongly constrained to align along the chain axis due to competition between interparticle interactions and the magnetic easy axis that is no longer parallel to the chain axis. This process will redistribute magnetic moments so that they are no longer along the chain axis, which will cause a remanence decrease (Figure 10a). A similar scenario is demonstrated by electron holography of magnetosome chains that indicate undulating magnetic induction lines near T_v [*Simpson et al*., 2005]. Upon warming across T_v, magnetite switches from its monoclinic phase back to the cubic phase where dipolar interactions cause the <111> easy axis to realign with the chain axis, rather than being randomly distributed (Figure 10a). During cooling-warming (above T_v - below T_v - above T_v; Figure 10a), dipolar interactions within magnetosome chains act like a spring, or a string through beads [*Simpson et al*., 2005]. LTC across T_v represents a perturbation of magnetosome chain systems that causes deviation of magnetic moments from (or oscillation along) the chain axis. However, dipolar interactions within the unique magnetosome chains restore the remanence due to the dipole spring mechanism.

[24] Without the dipole spring mechanism, the magnetic moment of isolated (Figure 10b) and clumped (Figure 10c) crystals would align with the nearest <111> easy axis that is not necessarily along a single direction upon warming through T_v. Alignment with the nearest <111> direction is expected for nearly equidimensional magnetite, but not for elongated magnetite particles with aspect ratios > 1.1. These processes for more equidimensional particles will produce more randomly distributed magnetic moments in space and will therefore result in a permanent remanence loss across T_v (Figures 10b and 10c). The dipole spring mechanism is only likely to affect samples containing intact magnetosome chains. Collapsed or clumped magnetosome chains would destroy the alignment needed for this mechanism. This probably explains why ultrasonicated AMB-1 cells have nonreversible cooling-warming curves, unlike intact AMB-1 samples before ultrasonication (Figure 7l). Ultrasonication of intact MTB samples cannot disrupt magnetite chains due to the constraints imposed by magnetosome membranes, but it can liberate magnetite crystals that are strung together in composite chains from different cells [*Kobayashi et al*., 2006; *Kopp et al*., 2006a]. Ultrasonication therefore can produce clumps with significant three-dimensional magnetostatic interactions that cause remanence loss. *Li et al*. [2013] reported reversible LTC curves for unoriented cells and field-aligned cells of MTB strain AMB-1, but irreversible curves for a remanence applied ~90° to the chain axis. In the case of remanence acquired 90° to the chain axis, the remanence is negligible in a collection of random axes, because the 90° remanence is much lower than that at a more shallow angle. In addition, the magnetic moments are not ideally aligned along the chain axis, unlike the situation depicted in Figure 10a. In such case, the dipole spring mechanism will not be as strong and the remanence will be partially lost during LTC treatment.

[25] The dipole spring model described here is also different from that of *Moskowitz et al*. [1993]. *Moskowitz et al*. [1993] invoked preferential selection of different crystallographic axes during FC and ZFC treatment to explain the difference in remanence loss during FC and ZFC measurements. In contrast, the dipole spring model provides an explanation for the reversibility of LTC curves and restoration of remanence. In the dipole spring model, a similar mechanism is invoked as the cause of reversible LTC behavior for isolated uniaxial stable SD particles (Figure 10d) [*Carter-Stiglitz et al*., 2004; *Muxworthy and Williams*, 2006], despite the fact that the fundamental interpretations at the microscale are different. This is not surprising because biogenic magnetite aligned in chains has many magnetic properties similar to those of other uniaxial stable SD assemblages [e.g., *Moskowitz et al*., 1993; *Egli et al*., 2010; *Charilaou et al*., 2011]. One consequence of this similarity is that reversible LTC curves are not uniquely indicative of intact biogenic magnetite chains because inorganic noninteracting uniaxial stable SD particles are also expected to produce such reversible LTC curves (see Figure 1 of *Carter-Stiglitz et al*. [2004]). This may cause potential ambiguity when seeking to identify biogenic magnetite within natural samples. Nonuniqueness is a common problem with nearly all rock-magnetic techniques, including the low-temperature ZFC/FC remanence test [*Moskowitz et al*., 1993], IRM decomposition [*Egli*, 2004a, 2004b], FMR spectroscopy [*Weiss et al*., 2004; *Kopp et al*., 2006a, 2006b; *Charilaou et al*., 2011], and FORC analysis [*Egli et al*., 2010]. Moreover, noninteracting uniaxial stable SD particles, which can be confused with intact biogenic magnetite chains, are relatively rare in natural environments. Confirmation of the presence of biogenic magnetite can require direct TEM observations. Nevertheless, our observations of biogenic magnetite and inorganic magnetic minerals suggest that reversible LTC cooling-warming curves (particularly nonmonotonic curves) can be used as a diagnostic indicator for the presence of intact magnetosome chains. Together with other magnetic tests, the method based on LTC experiments suggested here provides a powerful tool for identifying magnetosome chains. Compared to the low-temperature ZFC/FC magnetic test of *Moskowitz et al*. [1993], which is often affected by oxidation that suppresses the Verwey transition, the advantage of our suggested LTC treatment is that it is largely independent of the degree of oxidation. Oxidation can change the shapes of cooling and warming curves for biogenic magnetite chains, but it does not affect their reversibility. Other effects, such as mixed magnetic mineral assemblages, would also cause ambiguities if additional magnetic components undergo some degree of low-temperature demagnetization during

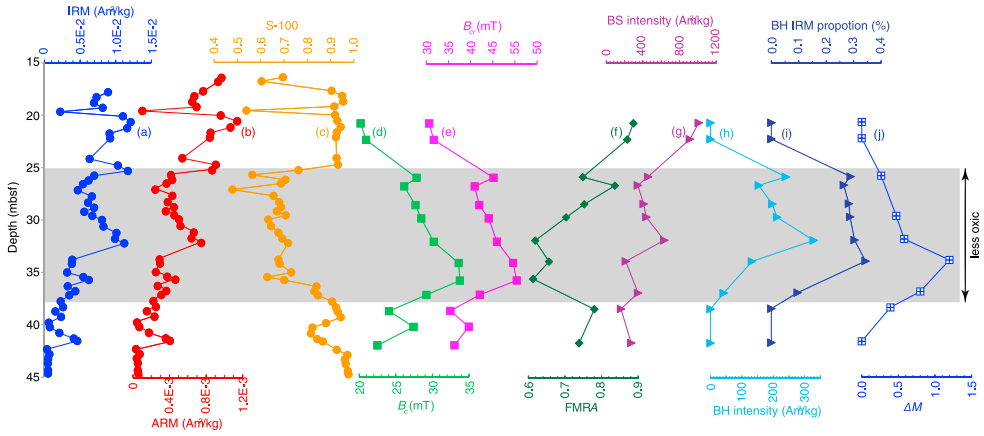

Figure 11. Magnetic parameter profiles for ODP Hole 738B: (a) IRM, (b) ARM, (c) S-100, (d) coercivity, B_c, (e) coercivity of remanence, B_{cr}, (f) FMR parameter A, (g) intensity of the BS component from IRM decomposition analysis, (h) intensity of the BH component from IRM decomposition analysis, (i) relative intensity of the BH component to the total IRM intensity, and (j) oxidation parameter, ΔM. The gray shading indicates the interval with higher B_c and B_{cr}, lower A, significant enrichment of a BH component, and novel low-temperature magnetic properties shown in Figures 3–5.

LTC treatment. These effects, however, are a common problem for most tests for biogenic magnetite, such as the *Moskowitz et al*. [1993] test and FMR analysis [*Weiss et al*., 2004]. Nevertheless, our results provide justification for an experimental method to identify biogenic magnetite in sediments that appears to be independent of the degree of oxidation, which in turn provides a complementary tool to previous approaches that will assist with achieving more robust identification of biogenic magnetite.

4.4. Environmental Implications of the Magnetic Record From ODP Hole 738B

[26] To aid interpretation of potential environmental magnetic records of pelagic carbonates, we present profiles of a range of rock magnetic properties for ODP Hole 738B (Figure 11). The magnetic properties of these sediments are dominated by biogenic magnetite [*Roberts et al*., 2011a]. An interval is identified between ~25 and 38 mbsf with distinct magnetic properties (shaded in Figure 11). Within this interval, magnetic concentration-dependent parameters (i.e., IRM and anhysteretic remanent magnetization (ARM)) generally increase up-core (Figures 11a and 11b), which indicates a general increase in MTB populations. Samples from this interval have relatively lower S-100 ratios (where S-100 represents the ratio between a back-field IRM at 100 mT and the SIRM; Figure 11c), high coercivity values (B_c and B_{cr}) (Figures 11d and 11e), and lower values of the FMR parameter A (Figure 11f). For biogenic magnetite, higher coercivity values indicate a stronger magnetic anisotropy. Lower values of A reflect more asymmetric FMR spectra, which also indicate increased shape anisotropy of biogenic magnetite [e.g., *Weiss et al*., 2004; *Kopp et al*., 2006a, 2006b; *Charilaou et al*., 2011; *Chang et al*., 2012b]. In addition, B_c and B_{cr} and A are inversely correlated. These results indicate enhanced magnetic anisotropy due to magnetosome chains, and the presence of a significant BH component within this stratigraphic interval. Our data also indicate that FMR spectroscopy potentially provides an excellent tool for detection of biogenic magnetite morphology, i.e., BS *vs* BH components. A relationship between increased coercivity and morphology of biogenic magnetite has previously been demonstrated [*Yamazaki and Ikehara*, 2012]. We therefore apply IRM decomposition analysis [*Kruiver et al*., 2001; *Heslop et al*., 2002] to separate the BS and BH components [*Egli*, 2004a, 2004b]. Our results indicate significant enhancement of the BH component during this interval (both in its absolute (Figure 11h) and relative abundance with respect to the BS component (Figure 11i)). On the other hand, the BS intensity (Figure 11g) increases up-section. The BS component is much stronger than the BH component; therefore, its stratigraphic variations should dominate the bulk IRM curve. Samples from this interval also have novel low-temperature magnetic properties (Figures 4 and 5). As discussed earlier, these low-temperature magnetic properties reflect partial oxidation of biogenic magnetite chains. Higher ΔM values correlate with higher coercivity and lowest FMR A values (Figure 11j), and therefore with BH content.

[27] To reconcile room temperature hysteresis, IRM curves, FMR spectra, and low-temperature magnetic properties, the interval from ODP Hole 738B with enigmatic magnetic properties can be explained by an enrichment of a less oxidized biogenic magnetite and BH component compared to samples from other intervals. Co-occurrence of less oxidation and elongated BH morphologies could be due to less oxic sedimentary environments. What was the environmental cause of this bacterial ecological shift? The factors that control the distribution of MTB communities are complex. For example, certain MTB species can spontaneously biomineralize both magnetite and greigite magnetosomes [e.g., *Bazylinski et al*., 1995]. Additionally, similar magnetosome crystals can be produced by many different MTB strains. However, a generally positive correlation between elongated magnetosomes and increased productivity has also been inferred from several Quaternary marine sediment records [e.g., *Hesse*, 1994; *Lean and McCave*, 1998; *Yamazaki and Kawahata*, 1998; *Yamazaki*, 2012; *Yamazaki and Ikehara*, 2012]. *Yamazaki* [2012]

observed that the BS component prevails during suboxic conditions and disappears during anoxic events, whereas the BH component is more resistant to anoxic conditions. *Hesse* [1994] reported similar cyclic glacial-interglacial changes in magnetofossil morphology in Tasman Sea sediments. In the case of ODP Hole 738B, *Roberts et al*. [2011a] argued that delivery of eolian dust increased surface ocean productivity, as suggested by a shift in nannofossil assemblages that are indicative of nutrient-poor to nutrient-rich conditions [*Persico et al*., 2011]. This productivity event is argued to have given rise to increased organic carbon burial that enabled increased magnetite biomineralization by MTB [*Roberts et al*., 2011a]. Our rock magnetic measurements support this conclusion that less oxic conditions associated with increased organic carbon burial prevailed during this part of the late Eocene at Site 738.

5. Conclusions

[28] Low-temperature magnetic analyses of pelagic carbonates and whole MTB cells enable documentation of a range of magnetic properties for biogenic magnetite. These properties can be largely explained by the degree of oxidation from a fully oxidized end-member to fresh magnetite. Nevertheless, our knowledge of the detailed mechanisms is incomplete. For example, much of the observed low-temperature magnetic behavior of oxidized biogenic magnetite, i.e., humped LTC curves, cannot be explained by a simple core-shell model. It is possible that oxidation throughout magnetite crystals is not homogenous with a continuous change in oxidation degree.

[29] We document novel low-temperature magnetic properties for marine carbonates, where SIRM warming curves undergo a broad decrease and LTC RTSIRM curves have a hump-like shape that is reversible during both cooling and warming. We interpret these properties to be due to partial oxidation of biogenic magnetite crystals and a dipole spring mechanism that acts within intact biogenic magnetite chains to stabilize and restore remanence across T_v. Reversible LTC cooling-warming curves can be used as a diagnostic feature to indicate potentially intact magnetosome chains within samples. Compared to the low-temperature test of *Moskowitz et al*. [1993] that uses ZFC/FC SIRM warming, the suggested LTC experiments for identifying biogenic magnetite chains have the advantage of being insensitive to oxidation of biogenic magnetite. As is the case for other magnetic techniques, the LTC protocol for biogenic magnetite identification has an inherent degree of nonuniqueness. For example, the presence of noninteracting uniaxial stable SD particles may cause interpretational ambiguities. Therefore, additional rock magnetic analyses or TEM observations could be needed to confirm the presence of biogenic magnetite.

[30] ODP Hole 738B contains an interval where the magnetic properties can be explained by less oxidation of biogenic magnetite and a significant enrichment of the BH component. These environmental magnetic signatures are likely associated with less oxic conditions and increased delivery of organic carbon to the seafloor. Such conditions would have lengthened the pathway for postdepositional oxygen diffusion into the sediment, which would have helped to preserve more pristine biogenic magnetite. Magnetic measurements provide a sensitive tool for characterizing marine carbonates, which can be used to obtain important paleoenvironmental information, particularly concerning oceanic productivity and oxygenation states.

[31] **Acknowledgments.** Pelagic carbonate samples were provided by the IODP, which is sponsored by the U.S. National Science Foundation and participating countries under management of the Joint Oceanographic Institutions, Inc. We thank Dirk Schüler, Ludwig-Maximilians University, Munich, for providing the cultured *Magnetospirillum gryphiswaldense* MSR-1 sample. Barbara Maher from Lancaster University is thanked for providing the synthetic magnetite sample. We thank Bob Kopp from Rutgers University and Jinhua Li from the Chinese Academy of Sciences, Beijing, for providing their published low-temperature magnetic data and TEM images for AMB-1 and MYR-1, respectively. We are grateful to Bruce Moskowitz, an associate editor, and an anonymous reviewer for their constructive comments, and André Revil for editorial handling.This work was partially supported by the Netherlands Organization for Scientific Research (NWO), the Australian Research Council (DP120103952), and the Japan Society for the Promotion of Science (JSPS).

References

Abrajevitch, A., and K. Kodama (2009), Biochemical vs. detrital mechanism of remanence acquisition in marine carbonates: A lesson from the K-T boundary interval, *Earth Planet. Sci. Lett.*, *286*, 269–277.

Bazylinski, D. A., R. B. Frankel, B. R. Heywood, S. Mann, J. W. King, P. L. Donaghay, and A. K. Hanson (1995), Controlled biomineralization of magnetite (Fe_3O_4) and greigite (Fe_3S_4) in a magnetotactic bacterium, *Appl. Environ. Microbiol.*, *61*, 3232–3239.

Bickford, L. R., J. M. Brownlow, and R. F. Penoyer (1957), Magnetocrystalline anisotropy in cobalt-substituted magnetic single crystals, *Proc. IEE .B*, *104*, 238–244.

Carter-Stiglitz, B., M. Jackson, and B. Moskowitz (2002), Low-temperature remanence in stable single domain magnetite, *Geophys. Res. Lett.*, *29*(7), 1129, doi:10.1029/2001GL014197.

Carter-Stiglitz, B., B. Moskowitz, and M. Jackson (2004), More on the low-temperature magnetism of stable single domain magnetite: Reversibility and nonstoichiometry, *Geophys. Res. Lett.*, *31*, L06606, doi:10.1029/2003GL019155.

Chang, L., A. P. Roberts, A. R. Muxworthy, Y. Tang, Q. Chen, C. J. Rowan, Q. Liu, and P. Pruner (2007), Magnetic characteristics of synthetic pseudo-single-domain and multi-domain greigite (Fe_3S_4), *Geophys. Res. Lett.*, *34*, L24304, doi:10.1029/2007GL032114.

Chang, L., A. P. Roberts, Y. Tang, B. D. Rainford, A. R. Muxworthy, and Q. Chen (2008), Fundamental magnetic parameters from pure synthetic greigite (Fe_3S_4), *J. Geophys. Res.*, *113*, B06104, doi:10.1029/2007JB005502.

Chang, L., A. P. Roberts, C. J. Rowan, Y. Tang, P. Pruner, Q. Chen, and C. S. Horng (2009), Low-temperature magnetic properties of greigite (Fe_3S_4), *Geochem. Geophys. Geosyst.*, *10*, Q01Y04, doi:10.1029/2008GC002276.

Chang, L., A. P. Roberts, W. Williams, J. D. Fitz Gerald, J. C. Larrasoaña, L. Jovane, and A. R. Muxworthy (2012a), Giant magnetofossils and hyperthermal events, *Earth Planet. Sci. Lett.*, *351–352*, 258–269, doi:10.1016/j.epsl.2012.07.031.

Chang, L., M. Winklhofer, A. P. Roberts, M. J. Dekkers, C.-S. Horng, L. Hu, and Q. W. Chen (2012b), Ferromagnetic resonance characterization of greigite (Fe_3S_4), monoclinic pyrrhotite (Fe_7S_8) and non-interacting titanomagnetite ($Fe_{3-x}Ti_xO_4$), *Geochem. Geophys. Geosyst.*, *13*, Q05Z41, doi:10.1029/2012GC004063.

Channell, J. E. T., C. Ohneiser, Y. Yamamoto, and M. S. Kesler (2013), Oligocene-Miocene magnetic stratigraphy carried by biogenic magnetite at sites U1334 and U1335 (equatorial Pacific Ocean), *Geochem. Geophys. Geosyst.*, *14*, 265–282, doi:10.1029/2012GC004429.

Charilaou, M., M. Winklhofer, and A. U. Gehring (2011), Simulation of ferromagnetic resonance spectra of linear chains of magnetite nanocrystals, *J. Appl. Phys.*, *109*, 093903, doi:10.1063/1.3581103.

Cui, Y., K. L. Verosub, and A. P. Roberts (1994), The effect of low-temperature oxidation on large multi-domain magnetite, *Geophys. Res. Lett.*, *21*, 757–760.

Dunin-Borkowski, R. E., M. R. McCartney, R. B. Frankel, D. A. Bazylinski, M. Posfai, and P. R. Buseck (1998), Magnetic microstructure of magnetotactic bacteria by electron holography, *Science*, *282*, 1868–1870.

Egli, R. (2004a), Characterization of individual rock magnetic components by analysis of remanence curves: 1. Unmixing natural sediments, *Stud. Geophys. Geod.*, *48*, 391–446, doi:10.1023/B:SGEG.0000020839.45304.6d.

Egli, R. (2004b), Characterization of individual rock magnetic components by analysis of remanence curves. 2. Fundamental properties of coercivity distributions, *Phys. Chem. Earth*, *29*, 851–867.

Egli, R., A. P. Chen, M. Winklhofer, K. P. Kodama, and C.-S. Horng (2010), Detection of noninteracting single domain particles using first-order reversal curve diagrams, *Geochem. Geophys. Geosyst.*, *11*, Q01Z11, doi:10.1029/2009GC002916.

Fischer, A., M. Schmitz, B. Aichmayer, P. Fratzl, and D. Faivre (2011), Structural purity of magnetite nanoparticles in magnetotactic bacteria, *J. R. Soc. Interface*, *8*, 1011–1018.

Fischer, H., G. Mastrogiacomo, J. F. Löffler, R. J. Warthmann, P. G. Weidler, and A. U. Gehring (2008), Ferromagnetic resonance and magnetic characteristics of intact magnetosome chains in *Magnetospirillum gryphiswaldense*, *Earth Planet. Sci. Lett.*, *270*, 200–208, doi:10.1016/j.epsl.2008.03.022.

Florindo, F., and A. P. Roberts (2005), Eocene-Oligocene magnetobiostratigraphy of ODP sites 689 and 690, Maud Rise, Weddell Sea, Antarctica, *Geol. Soc. Am. Bull.*, *117*, 46–66, doi:10.1130/B25541.1.

Hanzlik, M., M. Winklhofer, and N. Petersen (2002), Pulsed field-remanence measurements on individual magnetotactic bacteria, *J. Magn. Magn. Mater.*, *248*, 258–267, doi:10.1016/S0304-8853(02)00353-0.

Harrison, R. J., and J. M. Feinberg (2008), FORCinel: An improved algorithm for calculating first-order reversal curve distributions using locally weighted regression smoothing, *Geochem. Geophys. Geosyst.*, *9*, Q05016, doi:10.1029/2008GC001987.

Hartstra, R. L. (1982), A comparative study of the ARM and I_{sr} of some natural magnetites of MD and PSD grain size, *Geophys. J. R. Astron. Soc.*, *71*, 497–518.

Heslop, D., M. J. Dekkers, P. P. Kruiver, and I. H. M. van Oorschot (2002), Analysis of isothermal remanent magnetization acquisition curves using the expectation-maximization algorithm, *Geophys. J. Int.*, *148*, 58–64, doi:10.1046/j.0956-540x.2001.01558.x.

Hesse, P. P. (1994), Evidence for bacterial palaeoecological origin of mineral magnetic cycles in oxic and sub-oxic Tasman sea sediments, *Mar. Geol.*, *117*, 1–17.

Housen, B. A., and B. M. Moskowitz (2006), Depth distribution of magnetofossils in near-surface sediments from the Blake/Bahama Outer Ridge, western North Atlantic Ocean, determined by low-temperature magnetism, *J. Geophys. Res.*, *111*, G01005, doi:10.1029/2005JG000068.

Kim, B. Y., K. P. Kodama, and R. E. Moeller (2005), Bacterial magnetite produced in water column dominates lake sediment mineral magnetism: Lake Ely, USA, *Geophys. J. Int.*, *163*, 26–37, doi:10.1111/j.1365-246X.2005.02735.x.

Kobayashi, A., J. L. Kirschvink, C. Z. Nash, R. E. Kopp, D. A. Sauer, L. E. Bertani, W. F. Voorhout, and T. Taguchi (2006), Experimental observation of magnetosome chain collapse in magnetotactic bacteria: Sedimentological, paleomagnetic, and evolutionary implications, *Earth Planet. Sci. Lett.*, *245*, 538–550, doi:10.1016/j.epsl.2006.03.041.

Kopp, R. E., and J. L. Kirschvink (2008), The identification and biogeochemical interpretation of fossil magnetotactic bacteria, *Earth Sci. Rev.*, *86*, 42–61.

Kopp, R. E., C. Z. Nash, A. Kobayashi, B. P. Weiss, D. A. Bazylinski, and J. L. Kirschvink (2006a), Ferromagnetic resonance spectroscopy for assessment of magnetic anisotropy and magnetostatic interactions: A case study of mutant magnetotactic bacteria, *J. Geophys. Res.*, *111*, B12S25, doi:10.1029/2006JB004529.

Kopp, R. E., B. P. Weiss, A. C. Maloof, H. Vali, C. Z. Nash, and J. L. Kirschvink (2006b), Chains, clumps, and strings: Magnetofossil taphonomy with ferromagnetic resonance spectroscopy, *Earth Planet. Sci. Lett.*, *247*, 10–25.

Kruiver, P. P., M. J. Dekkers, and D. Heslop (2001), Quantification of magnetic coercivity components by the analysis of acquisition curves of isothermal remanent magnetization, *Earth Planet. Sci. Lett.*, *189*, 269–276, doi:10.1016/S0012-821X(01)00367-3.

Larrasoaña, J. C., A. P. Roberts, L. Chang, S. A. Schellenberg, J. D. Fitz Gerald, R. D. Norris, and J. C. Zachos (2012), Magnetotactic bacterial response to Antarctic dust supply during the Palaeocene-Eocene thermal maximum, *Earth Planet. Sci. Lett.*, *333–334*, 122–133, doi:10.1016/j.epsl.2012.04.003.

Lawver, L. A., and L. M. Gahagan (2003), Evolution of Cenozoic gateways in the circum-Antarctic region, *Palaeogeogr. Palaeoclimatol. Palaeoecol.*, *198*, 11–37.

Lean, C. M. B., and I. N. McCave (1998), Glacial to interglacial mineral magnetic and palaeoceanographic changes at Chatham Rise, SW Pacific Ocean, *Earth Planet. Sci. Lett.*, *163*, 247–260.

Li, J., Y. Pan, G. Chen, Q. Liu, L. Tian, and W. Lin (2009), Magnetite magnetosome and fragmental chain formation of *Magnetospirillum magneticum* AMB-1: Transmission electron microscopy and magnetic observations, *Geophys. J. Int.*, *177*, 33–42, doi:10.1111/j.1365-246X.2009.04043.x.

Li, J., et al. (2010), Biomineralization, crystallography and magnetic properties of bullet-shaped magnetite magnetosomes in giant rod magnetotactic bacteria, *Earth Planet. Sci. Lett.*, *293*, 368–376.

Li, J., W. Wu, Q. Liu, and Y. Pan (2012), Magnetic anisotropy, magnetostatic interactions and identification of magnetofossils, *Geochem. Geophys. Geosyst.*, *13*, Q10Z51, doi:10.1029/2012GC004384.

Li, J., K. Ge, Y. Pan, W. Williams, Q. Liu, and H. Qin (2013), A strong angular dependence of magnetic properties of magnetosome chains: Implications for rock magnetism and paleomagnetism, *Geochem. Geophys. Geosyst.*, *14*, doi:10.1002/ggge.20228.

Lowrie, W., and F. Heller (1982), Magnetic properties of marine limestones, *Rev. Geophys.*, *20*, 171–192.

Lowrie, W., J. E. T. Channell, and W. Alvarez (1980), A review of magnetic stratigraphy investigations in Cretaceous pelagic carbonate rocks, *J. Geophys. Res.*, *85*, 3597–3605, doi:10.1029/JB085iB07p03597.

Maher, B. A. (1988), Magnetic properties of some synthetic sub-micron magnetites, *Geophys. J. Int.*, *94*, 83–96, doi:10.1111/j.1365-246X.1988.tb03429.x.

Maloof, A. C., R. E. Kopp, J. P. Grotzinger, D. A. Fike, T. Bosak, H. Vali, P. M. Poussart, B. P. Weiss, and J. L. Kirschvink (2007), Sedimentary iron cycling and the origin and preservation of magnetization in platform carbonate muds, Andros Island, Bahamas, *Earth Planet. Sci. Lett.*, *259*, 581–598, doi:10.1016/j.epsl.2007.05.021.

Mauritsch, H. J., and P. Turner (1975), The identification of magnetite in limestones using the low-temperature transition, *Earth Planet. Sci. Lett.*, *24*, 414–418.

Moskowitz, B. M., R. B. Frankel, and D. A. Bazylinski (1993), Rock magnetic criteria for the detection of biogenic magnetite, *Earth Planet. Sci. Lett.*, *120*, 283–300, doi:10.1016/0012-821X(93)90245-5.

Moskowitz, B. M., M. Jackson, and C. Kissel (1998), Low temperature magnetic behavior of titanomagnetites, *Earth Planet. Sci. Lett.*, *157*, 141–149, doi:10.1016/S0012-821X(98)00033-8.

Moskowitz, B. M., D. A. Bazylinski, R. Egli, R. B. Frankel, and K. J. Edwards (2008), Magnetic properties of marine magnetotactic bacteria in a seasonally stratified coastal pond (Salt Pond, MA, USA), *Geophys. J. Int.*, *174*, 75–92, doi:10.1111/j.1365-246X.2008.03789.x.

Muxworthy, A. R., and E. McClelland (2000), Review of the low temperature magnetic properties of magnetite from a rock magnetic perspective, *Geophys. J. Int.*, *140*, 101–114.

Muxworthy, A. R., and W. Williams (2006), Low-temperature cooling behavior of single-domain magnetite: Forcing of the crystallographic axes and interactions, *J. Geophys. Res.*, *111*, B07103, doi:10.1029/2006JB004298.

Muxworthy, A. R., D. J. Dunlop, and Ö. Özdemir (2003), Low-temperature cycling of isothermal and anhysteretic remanence: Microcoercivity and magnetic memory, *Earth Planet. Sci. Lett.*, *205*, 173–184, doi:10.1016/S0012-821X(02)01039-7.

Özdemir, Ö., and D. J. Dunlop (2010), Hallmarks of maghemitization in low-temperature remanence cycling of partially oxidized magnetite nanoparticles, *J. Geophys. Res.*, *115*, B02101, doi:10.1029/2009JB006756.

Özdemir, Ö., D. J. Dunlop, and B. M. Moskowitz (1993), The effect of oxidation on the Verwey transition in magnetite, *Geophys. Res. Lett.*, *20*, 1671–1674, doi:10.1029/93GL01483.

Pan, Y., N. Petersen, A. F. Davila, L. Zhang, M. Winklhofer, Q. Liu, M. Hanzlik, and R. Zhu (2005a), The detection of bacterial magnetite in recent sediments of Lake Chiemsee (southern Germany), *Earth Planet. Sci. Lett.*, *232*, 109–123, doi:10.1016/j.epsl.2005.01.006.

Pan, Y., N. Petersen, M. Winklhofer, A. F. Davila, Q. Liu, T. Frederichs, M. Hanzlik, and R. Zhu (2005b), Rock magnetic properties of uncultured magnetotactic bacteria, *Earth Planet. Sci. Lett.*, *237*, 311–325, doi:10.1016/j.epsl.2005.06.029.

Passier, H. F., and M. J. Dekkers (2002), Iron oxide formation in the active oxidation front above sapropel S1 in the eastern Mediterranean Sea as derived from low-temperature magnetism, *Geophys. J. Int.*, *150*, 230–240, doi:10.1046/j.1365-246X.2002.01704.x.

Peck, J. A., and J. W. King (1996), Magnetofossils in the sediment of Lake Baikal, Siberia, *Earth Planet. Sci. Lett.*, *140*, 159–172, doi:10.1016/0012-821X(96)00027-1.

Penninga, I., H. de Waard, B. M. Moskowitz, D. A. Bazylinski, and R. B. Frankel (1995), Remanence measurements on individual magnetotactic bacteria using a pulsed magnetic field, *J. Magn. Magn. Mater.*, *149*, 279–286.

Persico, D., C. Fioroni, and G. Villa (2011), A refined calcareous nannofossil biostratigraphy for the Middle Eocene-Early Oligocene Southern Ocean ODP sites, *Palaeogeogr. Palaeoclimatol. Palaeoecol.*, *335–336*, 12–23, doi:10.1016/j.paleo.2011.05.017.

Pike, C. R., A. P. Roberts, and K. L. Verosub (1999), Characterizing interactions in fine magnetic particle systems using first order reversal curves, *J. Appl. Phys.*, *85*, 6660–6667, doi:10.1063/1.370176.

Prozorov, R., T. Prozorov, S. K. Mallapragada, B. Narasimhan, T. J. Williams, and D. A. Bazylinski (2007), Magnetic irreversibility and the Verwey transition in nanocrystalline bacterial magnetite, *Phys. Rev. B*, *76*, 054406, doi:10.1103/PhysRevB.76.054406.

Roberts, A. P., C. R. Pike, and K. L. Verosub (2000), First order reversal curve diagrams: A new tool for characterizing the magnetic properties of natural samples, *J. Geophys. Res.*, *105*, 28,461–28,475, doi:10.1029/2000JB900326.

Roberts, A. P., F. Florindo, G. Villa, L. Chang, L. Jovane, S. M. Bohaty, J. C. Larrasoaña, D. Heslop, and J. D. Fitz Gerald (2011a), Magnetotactic bacterial abundance in pelagic marine environments is limited by organic carbon flux and availability of dissolved iron, *Earth Planet. Sci. Lett.*, *310*, 441–452, doi:10.1016/j.epsl.2011.08.011.

Roberts, A. P., L. Chang, C. J. Rowan, C.-S. Horng, and F. Florindo (2011b), Magnetic properties of sedimentary greigite (Fe_3S_4): An update, *Rev. Geophys.*, *49*, RG1002, doi:10.1029/2010RG000336.

Roberts, A. P., L. Chang, D. Heslop, F. Florindo, and J. C. Larrasoaña (2012), Searching for single domain magnetite in the "pseudo-single-domain" sedimentary haystack: Implications of biogenic magnetite preservation for sediment magnetism and relative paleointensity determinations, *J. Geophys. Res.*, *117*, B08104, doi:10.1029/2012JB009412.

Roberts, A. P., F. Florindo, L. Chang, D. Heslop, L. Jovane, and J. C. Larrasoaña (2013), Magnetic properties of pelagic marine carbonates, *Earth Sci. Rev.*, *127*, 111–139, doi:10.1016/j.earscirev.2013.09.009.

Scheffel, A., A. Gärdes, K. Grünberg, G. Wanner, and D. Schüler (2008), The major magnetosome proteins MamGFDC are not essential for magnetite biomineralization in *Magnetospirillum gryphiswaldense*, but regulate the size of magnetosome crystals, *J. Bacteriol.*, *190*, 377–386.

Schüler, D., and M. Köhler (1992), The isolation of a new magnetic spirillum, *Zentralbl. Mikrobiol.*, *147*, 150–151.

Simpson, E. T., T. Kasama, M. Pósfai, P. R. Buseck, R. J. Harrison, and R. E. Dunin-Borkowski (2005), Magnetic induction mapping of magnetite chains in magnetotactic bacteria at room temperature and close to the Verwey transition using electron holography, *J. Phys.: Conf. Ser.*, *17*, 108–121.

Smirnov, A. V., and J. A. Tarduno (2000), Low-temperature magnetic properties of pelagic sediments (Ocean Drilling Program Site 805C): Tracers of maghemitization and magnetic mineral reduction, *J. Geophys. Res.*, *105*, 16,457–16,471, doi:10.1029/2000JB900140.

Tarduno, J. A. (1994), Temporal trends of magnetic dissolution in the pelagic realm: Gauging paleoproductivity?, *Earth Planet. Sci. Lett.*, *123*, 39–48, doi:10.1016/0012-821X(94)90255-0.

Tarduno, J. A. (1995), Superparamagnetism and reduction diagenesis in pelagic sediments: Enhancement or depletion?, *Geophys. Res. Lett.*, *22*, 1337–1340, doi:10.1029/95GL00888.

Tarduno, J. A., W. L. Tian, and S. Wilkison (1998), Biogeochemical remanent magnetization in pelagic sediments of the western equatorial Pacific Ocean, *Geophys. Res. Lett.*, *25*, 3987–3990, doi:10.1029/1998GL900079.

Torii, M. (1997), Low-temperature oxidation and subsequent downcore dissolution of magnetite in deep-sea sediments, ODP Leg 161 (western Mediterranean), *J. Geomagn. Geoelectr.*, *49*, 1233–1245.

Valet, J.-P., and L. Meynadier (1993), Geomagnetic field intensity and reversals during the past four million years, *Nature*, *366*, 91–95.

Vali, H., O. Förster, G. Amarantidis, and N. Petersen (1987), Magnetotactic bacteria and their magnetofossils in sediments, *Earth Planet. Sci. Lett.*, *86*, 389–400, doi:10.1016/0012-821X(87)90235-4.

van Velzen, A. J., and J. D. A. Zijderveld (1990), Rock magnetism of the early Pliocene Trubi formation at Eraclea Minoa (Sicily), *Geophys. Res. Lett.*, *17*, 791–794.

Verwey, E. J. W. (1939), Electronic conduction of magnetite (Fe_3O_4) and its transition point at low temperatures, *Nature*, *144*, 327–328.

Walz, F. (2002), The Verwey transition - A topical review, *J. Phys. Condens. Matter*, *14*, R285–R340, doi:10.1088/0953-8984/14/12/203.

Weiss, B. P., S. S. Kim, J. L. Kirschvink, R. E. Kopp, M. Sankaran, A. Kobayashi, and A. Komeili (2004), Ferromagnetic resonance and low temperature magnetic tests for biogenic magnetite, *Earth Planet. Sci. Lett.*, *224*, 73–89.

Yamazaki, T. (2009), Environmental magnetism of Pleistocene sediments in the North Pacific and Ontong-Java Plateau: Temporal variations of detrital and biogenic components, *Geochem. Geophys. Geosyst.*, *10*, Q07Z04, doi:10.1029/2009GC002413.

Yamazaki, T. (2012), Paleoposition of the intertropical convergence zone in the eastern Pacific inferred from glacial-interglacial changes in terrigenous and biogenic magnetic mineral fractions, *Geology*, *40*, 151–154.

Yamazaki, T., and M. Ikehara (2012), Origin of magnetic mineral concentration variation in the Southern Ocean, *Paleoceanography*, *27*, PA2206, doi:10.1029/2011PA002271.

Yamazaki, T., and N. Ioka (1997), Environmental rock magnetism of pelagic clay: Implications for Asian eolian input to the North Pacific since the Pliocene, *Paleoceanography*, *12*, 111–124.

Yamazaki, T., and H. Kawahata (1998), Organic carbon flux controls the morphology of magnetofossils in marine sediments, *Geology*, *26*, 1064–1066.

Yamazaki, T., and P. Solheid (2011), Maghemite-to-magnetite reduction across the Fe-redox boundary in a sediment core from the Ontong-Java Plateau: Influence on relative palaeointensity estimation and environmental magnetic application, *Geophys. J. Int.*, *185*, 1243–1254, doi:10.1111/j.1365-246X.2011.05021.x.

Yamazaki, T., A. L. Abdeldayem, and K. Ikehara (2003), Rock-magnetic changes with reduction diagenesis in Japan Sea sediments and preservation of geomagnetic secular variation in inclination during the last 30,000 years, *Earth Planets Space*, *55*, 327–340.